

## Characteristics of plasma flows at the inner edge of the plasma sheet

R. L. McPherron,<sup>1</sup> T.-S. Hsu,<sup>1</sup> J. Kissinger,<sup>1</sup> X. Chu,<sup>1</sup> and V. Angelopoulos<sup>1</sup>

Received 11 July 2010; revised 22 December 2010; accepted 6 January 2011; published 19 April 2011.

[1] All known types of auroral zone magnetic activity are associated with closure of open magnetic flux in the magnetotail. As closure is caused by magnetic reconnection we expect to observe fast flows during geomagnetic activity. We have scanned the ion flow data during the first pass of the THEMIS D spacecraft through the tail (December 2007 to May 2008), identifying all flows with  $|V_{\perp x}| > 150$  km/s. These flows generally occur in a sequence of several short bursts (bursty bulk flows). Earthward flows are much more common than tailward flows and are faster than tailward flows. Earthward flows have a longer duration; tailward flows are seen alone or after an earthward flow. Both directions of flow are associated with an increase in tail  $B_z$  (dipolarization). Fast flows in either direction are rarely seen inside of  $9 R_E$ . Earthward flows are strongly localized in the local time sector 2100–0100 and have a probability distribution identical to that seen in auroral substorm expansions by the IMAGE spacecraft. Tailward flows are also localized but with a peak shifted to 2330 LT. Very close to midnight the flows are slowed and reflected. At other local times they appear to be deflected around the Earth. Fast flows often follow a reduction in  $E_s$  (GSM  $VB_s$ ) and occur close to the time of a sudden decrease in the  $AL$  index. Generally, the first flow burst in a sequence is most closely associated with the  $AL$  onset, and its peak follows the  $AL$  onset by about 2 min. The probability of observing a fast flow at THEMIS D during steady magnetospheric convection (SMC) events is quite low compared with the probability during an interval before the SMC. Since most of the fast flows carry magnetic flux earthward and are associated with substorm onset seen in the aurora by IMAGE and in the  $AL$  index, we interpret them as evidence that magnetic reconnection has occurred in the tail. Near  $30 R_E$  in the tail plasmoid ejection has also been associated with substorm onset, so we conclude that the fast flows are created by a new X line formed outside the 11.9 apogee of THEMIS D some time earlier than they are seen at THEMIS D. During SMC it appears that fast flows due to reconnection are deflected around the Earth outside the apogee of the satellite.

**Citation:** McPherron, R. L., T.-S. Hsu, J. Kissinger, X. Chu, and V. Angelopoulos (2011), Characteristics of plasma flows at the inner edge of the plasma sheet, *J. Geophys. Res.*, 116, A00I33, doi:10.1029/2010JA015923.

### 1. Introduction

[2] The magnetosphere responds to the solar wind in a variety of ways depending on the strength and waveform of the interplanetary magnetic field (IMF), the dynamic pressure and Mach number of the solar wind, and the electrical conductivity of the northern and southern ionospheres. Several distinct modes of response have been identified including pseudo breakups [Akasofu, 1964; Voronkov *et al.*, 2003], substorm expansion onsets [Ohtani *et al.*, 1999], intensifications of the expansion [Wiens and Rostoker, 1975], poleward boundary intensifications [de la Beaujardiere *et al.*, 1994], convection bays [Pytte *et al.*, 1978] or steady magnetospheric

convection (SMC) [Sergeev *et al.*, 1996], and sawtooth events [Borovsky *et al.*, 2001; Henderson *et al.*, 2006]. All of these phenomena are associated with southward IMF and each has been shown to be correlated with the closure of open magnetic flux in the tail lobes [Hubert *et al.*, 2009; Milan *et al.*, 2008, and references therein]. The inescapable conclusion is that magnetic reconnection plays an essential role in each of these modes of response.

[3] In this paper we will examine the relation of plasma sheet flows to two of these modes of response: substorms and steady magnetospheric convection. The concept of a substorm was developed nearly 50 years ago [Akasofu, 1964; Chapman, 1962], and the physical processes responsible for a substorm are still a subject of considerable controversy. In brief a substorm is an organized response of the magnetosphere to the onset of an interval of dayside magnetic reconnection. Magnetic flux is eroded from the dayside and transported to the tail lobes. The plasma sheet responds to

<sup>1</sup>Institute of Geophysics and Planetary Physics and Department of Earth and Space Science, University of California, Los Angeles, California, USA.

the additional flux by thinning, moving earthward, and increasing the cross-tail current. After about 50 min of the growth of these effects the aurora at the equatorward edge of the auroral oval suddenly brightens and expands poleward. Associated with the auroral expansion the polar cap contracts as the flux stored in the tail lobes reconnects, and a portion of the inner edge of the tail current is diverted through the ionosphere. During the expansion phase and the following recovery phase magnetic flux is returned to the dayside by plasma flows in the near-Earth plasma sheet. The distinguishing features of a substorm are a difference in the dayside and nightside reconnection rates and the poleward expansion of auroral and magnetic activity.

[4] The concept of steady magnetospheric convection was introduced more recently. The phenomenon was initially reported by Pytte *et al.* [1978] who noted that during steady intervals of southward IMF the magnetosphere occasionally enters a state of elevated activity during which there is little change in magnetic configuration and no expansions of the aurora. The authors named this phenomenon “convection bay” because of the continuous disturbance in the *AE* indices without evidence of substorm expansions. It was postulated that convection bays are examples of balanced dayside and nightside reconnection during which there is no net change in the amount of open flux stored in the tail lobes. Sergeev *et al.* [1996] and coauthors renamed this phenomenon “steady magnetospheric convection (SMC)” and carried out extensive analysis of six events. Their analysis supported the hypothesis of balanced reconnection and suggested that reconnection on the nightside occurs at an X line formed by a preceding substorm expansion. It appears that the X line moves some distance tailward of its location during the substorm expansion and sporadically reconnects across a broad range of the tail creating channels of earthward flow. These are seen in the auroral oval as poleward boundary intensifications (PBI). The distinguishing features of SMC are elevated magnetic activity, absence of poleward expansions, and a steady magnetospheric configuration.

[5] Today there is little argument that a southward IMF connects to the Earth’s magnetic field on the dayside opening magnetic flux [Baker *et al.*, 1996]. Newly opened magnetic flux is transported across the polar caps and temporarily stored in the lobes of the tail. The feet of the open field lines connect to the Earth in the polar caps. As open flux accumulates, the polar caps, defined as the dark regions poleward of the auroral ovals, expand equatorward. If dayside reconnection were to continue indefinitely all dayside magnetic flux would be opened and added to the polar caps. Besides this increase in size of the polar caps the magnetosphere responds in a variety of other ways including erosion of the magnetopause, a change in magnetopause shape, onset of sunward convection, earthward motion of the inner edge of the plasma sheet, and plasma sheet thinning. Eventually these changes lead to the onset of magnetic reconnection in the tail and open flux is closed. Once closed the magnetic flux is transported to the dayside by flows in the plasma sheet. Each of the response modes mentioned above is a different manifestation of the manner in which tail reconnection occurs. Thus, the primary purpose of geomagnetic activity is to return magnetic flux to the dayside of the magnetosphere.

[6] It was established previously that plasma flows in the tail are bursty and localized in narrow channels [Angelopoulos

*et al.*, 1992, 1994, 1996]. Earthward plasma velocities up to several hundred kilometers per second are frequently seen in the plasma sheet beyond  $10 R_E$ . These flows occur in narrow channels of a few Earth radii ( $R_E$ ) width. As these flows penetrate the inner magnetosphere they slow down as they enter regions of increasing field strength according to the formula  $E = VB$ . If the electric field is constant throughout the plasma sheet and *B* increases from 5 to 100 nT there will be a 20-fold decrease in flow speed to a few tens of kilometers per second. This is the noise level of most previous plasma instruments and these flows are detectable only in long-term averages.

[7] Recently the THEMIS mission launched five spacecraft into synchronized orbits in the tail such that the spacecraft have orbital periods of 4 days (THEMIS B), 2 days (C), 1 day (D and E), and approximately 1 day (A) [Angelopoulos, 2008]. The orbits are phased so that a major conjunction (four spacecraft) occurs at apogee every 4 days and a minor conjunction every 2 days (two spacecraft). The line of apogees was chosen so that conjunctions in the midtail occur over North America in February and March of 2008 and 2009. Studies of magnetic activity requiring major conjunctions are limited by two factors. First, the conjunctions only last about 10 h out of every 96, and second, the outer spacecraft (B and C) are only in the plasma sheet about 1 out of 5 h. Together this gives about a 2% chance of catching an earthward flow at all spacecraft during conjunction.

[8] To alleviate the foregoing problem we have chosen to use the inner spacecraft THEMIS D wherever it is located to study the statistical properties of flows at the inner edge of the plasma sheet. Apogee for THEMIS D is at  $11.9 R_E$  in the heart of the region often referred to as the “current disruption” region [Lui, 1991, 1996]. We will show that the arrival of a fast flow, a sudden onset of fluctuations in the magnetic field, and a prolonged enhancement in  $B_z$  (dipolarization) are the characteristic signatures of substorms in this region. In this paper we investigate the properties of these flows, their spatial distribution, their relation to dipolarization, their association with the IMF, and their relation to magnetic activity as revealed by the *AL* index. We focus on two types of magnetic activity: substorms as defined by a sudden decrease in the *AL* index and steady magnetospheric convection as defined by a steady elevated *AE* index without sudden drops in the *AL* index.

## 2. Background

[9] Since the near-Earth neutral line model was developed to explain magnetospheric substorms [Hones, 1973; McPherron *et al.*, 1973; Nishida and Nagayama, 1973] there have been many attempts to prove that plasma flow direction and magnetic field orientation are correlated as expected from magnetic reconnection. One of the first statistical studies of this relation was reported by Caan *et al.* [1979]. Using 324 events measured on the IMP 6 spacecraft (apogee  $33.1 R_E$ ) the authors showed that  $B_z$  in tailward flows is biased toward negative values and in earthward flows toward positive values as predicted by reconnection theory. However, the observation of northward fields in tailward flows led them to speculate that the thin sheet tailward of the X line contains weak  $B_z$  and is susceptible to tilting and waving producing intervals of northward  $B_z$ . They

also speculated that multiple plasmoids produced by bursty reconnection could produce such a result. Surprisingly the  $AE$  index associated with the high-speed flows was only twice the quiet time values.

[10] The early work on magnetotail flows and fields was greatly extended by studies of the AMPTE IRM data [Baumjohann, 1988; Baumjohann *et al.*, 1988, 1989, 1990, 1991]. With an apogee of  $18.5 R_E$  and equatorial orbit plane the IRM spacecraft was able to explore the inner portion of the magnetotail. In Baumjohann *et al.* [1988] it was established that the plasma sheet boundary layer (PSBL) is a unique part of the plasma sheet subject to occasional bursts of high-speed, field-aligned flow, but having a relatively low average velocity. Baumjohann *et al.* [1989] examined the properties of the central plasma sheet. They determined that it also experiences bursty earthward fast flows of duration less than a minute and that it exhibits an average velocity comparable to that in the PSBL. Ion temperature increases and ion density decreases with increasing magnetic activity. The nearly complete absence of tailward flows with negative  $B_z$  led them to conclude that the near-Earth X line must form beyond  $19 R_E$ .

[11] Baumjohann *et al.* [1990] performed a detailed investigation of the properties of high-speed flow bursts ( $V > 400$  km/s). In all layers of the plasma sheet the probability of a specific high-speed is less than 1.4% and decreases exponentially with speed, and also decrease linearly with density. PSBL bursts of low speed are more common than central plasma sheet (CPS) flows but at high speed they are nearly equal. In the CPS the probability of a high-speed flow increases with  $AE$ , decreases to low values approaching the inner edge of the plasma sheet ( $X \sim -10 R_E$ ), and decreases rapidly away from midnight. High-speed flows usually last less than 10 s and almost never more than 60 s. Virtually all the high-speed flow inside  $19 R_E$  are directed earthward.

[12] An alternative to the neutral line model favored by Baumjohann and coworkers was postulated by Lui *et al.* [1988] from an examination of particle and field data from the AMPTE CCE, the sister spacecraft to IRM with apogee at  $8.8 R_E$ . In this region the authors found that the characteristic signature of substorm onset is the sudden appearance of fluctuations in the magnetic field and an increase in its  $Z$  component (dipolarization). The authors suggest that this region of turbulent magnetic field is the source of particles injected deeper into the magnetosphere and also the region from which current is diverted into the substorm current wedge. In a subsequent paper Lui *et al.* [1990] invoke the kinetic cross-field streaming instability as the cause of the magnetic turbulence. They argue that this instability disrupts the cross-tail current allowing stretched field lines to collapse in a “convective surge.” The diverted current creates the substorm current wedge and the observed increase in  $B_z$ . Additional details of this model are presented in a synthesis model [Lui, 1991]. In this synthesis it was suggested that all bursts of flow in the CPS are produced by current disruption events that trigger a collapse of extended field lines and a rarefaction wave that pulls plasma into the inner edge of the plasma sheet. It is only after several of these at progressively greater distances that a rarefaction wave triggers reconnection at a distant location. Plasma jets from this region are diverted into field-aligned flows in the PSBL. In this model

plasma flows are a consequence of current disruption (CD) not the cause.

[13] The detailed properties of individual flow bursts were investigated by Angelopoulos *et al.* [1992]. They found that the bursts were organized into  $\sim 10$  min intervals of enhanced flow speed within which there were short-duration bursts of very high speed. They introduced the name bursty bulk flow (BBF) to describe this phenomenon. Their analysis showed that the average burst is associated with a temporary decrease in  $B_x$  and increase in  $B_z$  (dipolarization) and also with an increase in ion temperature. It should be noted that this use of the term “dipolarization” refers to a temporary increase in  $B_z$  in contrast to the prolonged increase in  $B_z$  called dipolarization closer to the Earth. The bursts generally have a large component perpendicular to the magnetic field and are therefore carrying magnetic flux sunward. Their estimates show that if these bursts occupy a cross section of only  $(3 \times 3 R_E^2)$  they transport as much mass, momentum and energy as “steady convection” across the entire tail.

[14] Angelopoulos *et al.* [1994] extended the study of BBFs in the IRM data and compared the results to properties of BBFs found in ISEE-2 data. In total they identified 114 IRM events and 241 ISEE-2 events with peak velocities exceeding 400 km/s. They found that flows with these speeds rarely penetrate inside  $12 R_E$  and that tailward flows with southward  $B_z$  were almost nonexistent in the IRM data and occurred only rarely in ISEE data beyond  $17 R_E$ . They also found that the occurrence rate of BBFs increases from 6% to 18% as the  $AE$  index increases from  $\sim 50$  nT to 500 nT.

[15] The relation of high-speed flows and magnetic field dipolarization to substorm onset was examined by Baumjohann [1996] and Baumjohann *et al.* [1991] using superposed epoch analysis of IRM data. A set of 39 substorms with clear signatures in multiple indicators was selected. For each substorm the major onset was chosen as the reference time. The results show that in the CPS both dipolarization and high-speed flow are closely associated with substorm onset and reach a peak at the start of the recovery phase ( $\sim 45$  min). The ion temperature increases during the expansion phase while the density decreases. In the PSBL the flow speed increases as in the CPS, but the increase in  $B_z$  and temperature only occur in the recovery phase. In contrast to the Lui model the authors interpret dipolarization in the near-Earth region as the result of reconnection jets depositing newly closed magnetic flux at the inner edge of the plasma sheet.

[16] The development of the substorm current wedge via flux pileup was investigated experimentally by Shiokawa and colleagues in a series of papers [Shiokawa *et al.*, 1997, 1998a, 1998b, 1998c]. Shiokawa *et al.* [1997] point out that the deceleration of the flows by an inward pressure gradient will produce a dawnward inertial current. In addition the increase in magnetic field behind the dipolarization front (here defined as the leading edge of a flow burst) requires a dawnward current as well. Together these two currents partially cancel the cross-tail current in the pileup region requiring a diversion of a portion of the tail current to the ionosphere from the edges of the pileup. An estimate of the total strength of these currents shows they are insufficient to explain a typical current wedge [Shiokawa *et al.*, 1998a]. This concept was applied to an isolated substorm by

*Shiokawa et al.* [1998b] and shown to be consistent with observations. The data suggest that both the initial stage of formation of the substorm current wedge and Pi 2 pulsations are caused by the arrival of the flow burst. The authors argue that the pileup process is the solution to the problem found in the near-Earth neutral line model where auroral breakup projects along field lines to the current disruption region near  $10 R_E$  and not to the X line at  $25 R_E$  [Baker et al., 1996]. *Shiokawa et al.* [1998c] consider the cause of later stages of the substorm current wedge and suggested it is produced by an azimuthal pressure gradient created by the pileup of magnetic flux and plasma.

[17] The explanation of dipolarization by flux pileup was investigated theoretically with MHD simulations by *Birn and Hesse* [1991] and *Hesse and Birn* [1991]. They found that dipolarization is caused by compression of the magnetic field as flows come to a stop at the inner edge of the plasma sheet. Current disruption and diversion into field-aligned currents on the other hand occur tailward of the region of dipolarization but earthward of the X line and are primarily a consequence of flow vorticity. The pattern of the diverted currents in their simulations is the same as those inferred in the substorm current wedge. A greatly improved simulation of these processes including a dipole field, a more realistic tail configuration, and a thin current sheet is described by *Birn and Hesse* [1996]. They find that the current diversion is produced by deflected flows shearing the magnetic field of the plasma sheet relative to higher-latitude field lines, and by vertical pressure gradients in the same region. *Birn et al.* [1999] extend this work confirming the results of *Shiokawa et al.* [1997] that the inertial current is quite small and short-lived, but that vertical gradients are more important than azimuthal gradients as argued by *Shiokawa et al.* [1998a]. It should be emphasized that in the simulations resistivity in the current disruption region is not the cause of current disruption as postulated in the CD model.

[18] A detailed multipoint analysis of a single bursty bulk flow (BBF) event and its effects close to the Earth was reported by [Angelopoulos et al., 1996]. The authors conclude that a single BBF flowing in a very narrow channel ( $1-2 R_E$ ) is sufficient to account for all the energy dissipated in the inner magnetosphere and ionosphere during the duration of the BBF. They also found that the flow ceases when local dipolarization is complete. They postulate that this corresponds to the passage of a “dipolarization front” tailward over the spacecraft. According to this definition a dipolarization front is the boundary between taillike and more dipolar field.

[19] The study of dipolarization fronts mentioned above was extended to greater distances in a statistical study using Geotail data by *Baumjohann et al.* [1999, 2000]. The authors binned magnetic field and flow data in time relative to substorm onset and distance behind the Earth to determine the behavior of dipolarization. They showed that the times of dipolarization onset and peak  $B_z$  are progressively delayed from 11 to  $30 R_E$  indicating a slow outward motion of dipolarization. In addition they demonstrated that tailward flows are seen just after onset only beyond  $21 R_E$  and that these flows reverse when the dipolarization front reaches these locations. They interpret these results as evidence that bursty flows transport magnetic flux earthward where it piles up with an outer boundary that moves tailward with time. As

this boundary approaches the X line it chokes the flow either stopping reconnection or forcing it to move tailward. This result was predicted theoretically by the simulations discussed above.

[20] The concept of a “dipolarization front” is used differently by *Sergeev et al.* [1998] who describe the injection of particles deep in the magnetosphere as a combination of an “injection front” and a subsequent “dipolarization front” that moves inward at convective speeds. *Nakamura et al.* [2002] adopted this usage in a study of a flow burst seen at Cluster ( $R \sim 17 R_E$ ). They find that the flow burst is preceded by a  $\sim 2000$  km thick layer in which  $B_z$  increases rapidly. Ahead of this front plasma is diverted around the flow burst while behind it the high-speed flow is nearly parallel to the front. *Runov et al.* [2009] used five THEMIS spacecraft to describe observations of a dipolarization front preceding a BBF. Their results are unambiguous: The front is seen first at greatest distance and progressively later at spacecraft closer to the Earth. Far from the Earth ( $X < -16 R_E$ ) dipolarization is temporary while closer to the Earth ( $X \sim -12 R_E$ ) there is a prolonged increase in  $B_z$ .

[21] The idea that flow braking is the cause of a substorm expansion was questioned by *Ohtani et al.* [2002a] using Geotail data  $10 R_E$  behind the Earth. A case study of two nearly identical flow bursts observed in the “braking region” showed that one burst produced a pseudo breakup while the other produced a full expansion. In a companion paper *Ohtani et al.* [2002b] examined flow bursts that occurred at Geotail near  $X = -37 R_E$  during active intervals preceded and followed by at least an hour of quiet times. In one case there was an intense tailward flow and only weak activity at high latitudes. In the second case there was a very strong earthward flow and again little activity in the auroral zone. The authors conclude that flow braking alone is insufficient to generate a substorm expansion and that an additional process is required. *Ohtani* [2004] reiterate this theme arguing that many lobe reconnection and flow events do not develop into substorm expansions. Also they point out that poleward boundary intensifications produce flow bursts and auroral streamers, but no auroral features have been found to precede substorm onsets.

[22] A very extensive survey of fast flows with  $V_{\perp x} > 300$  km/s at Geotail was reported by *Ohtani et al.* [2004]. In the tail this survey identified 818 earthward and 290 tailward flow events at  $X > -31 R_E$ . These events were analyzed using superposed epoch analysis with two different reference times: the start of the fast flow and the start of the  $B_z$  increase. The median curves clearly show the following:  $B_z$  temporarily increases during the earthward flow; the dipolarization is usually preceded by a sharp decrease in  $B_z$  associated with a momentary increase in density; subsequent to the flow the density is at a lower level and  $B_z$  is at a higher level. These features are evident in all 5  $R_E$  bins between  $X = -5$  and  $-31 R_E$ . Similar results different only in details are found for tailward flows in the same distance range. The exception is that tailward flows close to the Earth almost never exhibit decreases in  $B_z$ . The authors conclude that “[t]he near-Earth reconnection is inferred to be the responsible mechanism for most, if not all, flow events.” In a subsequent paper *Ohtani et al.* [2006] considered the effects of the fast flows at geosynchronous orbit. They were unable to show any systematic relation between the dipolarization at

this location and fast flows at Geotail. From this negative result they concluded: “but it strongly suggests that the near-Earth reconnection, even if it is an important component of the tail substorm process, is not sufficient for triggering a substorm onset.”

[23] Very recently *Ohtani et al.* [2009] examined the characteristics of tailward flows in the near-Earth region defined as a box with limits  $|Y| < 5$  and  $-8 > X > -15 R_E$ . They found that tailward flows with  $V < -200$  km/s are almost as common as earthward flows in this region ( $\text{prob} = 0.8 \times 10^{-2}$  as compared to  $1.0 \times 10^{-2}$ ) and that almost all are associated with a positive change in  $B_z$  (98.6%), with an increase in temperature, and a decrease in density. These are the same characteristics found for earthward flow events. In the 3.5 years of data the authors found sixty-two 12 s samples with  $V < -200$  km/s. Applying the additional constraint that there is no such sample in the preceding 15 min reduced the list to 24 events. A superposed epoch analysis showed that the average tailward flow burst lasts about 1 min and is often preceded by an earthward flow. The authors consider and rule out several possible explanations for the tailward flow including reconnection earthward of the spacecraft, Kelvin-Helmholtz instability, and the interchange instability. Their most likely explanation is a “bounce-back effect” in which earthward flows penetrate too close to the Earth and are reflected tailward.

[24] In this paper we extend previous work on the nature of plasma flows earthward of  $X = -11.9 R_E$ . Data from THEMIS D during its first tail pass through the tail are examined to determine the statistical properties of the flows and also their relation to northward turnings, dipolarization, and substorm onset as defined by the  $AL$  index.

### 3. Database

[25] The data used in this investigation include solar wind plasma and magnetic field and magnetic indices at one minute resolution from the Omni file provided by the NSSDC, 3 s resolution fluxgate magnetometer data (FGM), and onboard moments of the ion distribution determined by the THEMIS electrostatic analyzers (ESA) both downloaded from the THEMIS mission database. The data were in daily Common Data Format (CDF) files with some missing or overlapping data at day boundaries. These anomalies were eliminated producing complete daily files with 28,800 records per day in ASCII format. The magnetometer data was used to determine the field-aligned and perpendicular components of the flow velocity in GSM coordinates. All data during the 2008 tail pass were then written into two Matlab binary files containing plasma and magnetic field data. These files provide the ability to randomly access any data interval needed in subsequent analysis.

### 4. Analysis Methods

[26] The data analysis included several steps. The first step was to automatically detect fast flows ( $V_{\perp} > 150$  km/s) along the GSM  $x$  axis. This was done by identifying the start and stop times of all intervals in which  $V_{\perp x}$  was either greater than this threshold value or less than its negative. Each interval was processed to determine the time of maximum  $\text{abs}(V_{\perp x})$ . These times, the peak flow speed, and the

GSM location of the spacecraft were written to a file for later use. A second step displayed a 14 h plot containing  $AU$ ,  $AL$ ,  $AE$ ,  $\text{abs}(\langle d(AL)/dt \rangle)$ ,  $\langle \text{std}(AL) \rangle / \langle AL \rangle$ , and  $\text{prob}(\text{SMC})$ . An example plot is presented in Figure 1. Angular brackets indicate a 15 min running average. The probability that a given point is an SMC was calculated from the number of points that satisfy the SMC selection criteria in a 90 min moving window. These criteria included:  $AU > 50$  nT;  $AL < -75$  nT; and  $-25 < d(AL)/dt < +10$  nT/min. This plot was examined and all sharp breaks in the slope of the  $AL$  index characteristic of a negative bay were selected. Three onsets are shown in Figure 1 by vertical dashed lines. The selected times were written to a file as an “initial estimate” of substorm onset times. Without further information we cannot determine whether these correspond to pseudo breakups, true expansion onsets, intensifications or poleward boundary intensifications (PBI). In a second pass of this program with the same parameters the start and stop times of possible SMC events were selected visually. The parameter  $\text{prob}(\text{SMC})$  was used as a guide, but the start and stop times were visually selected to correspond to intervals when the  $AL$  index had partially recovered from a substorm expansion and was exhibiting a nearly constant value for more than 90 min. The start and stop times of the SMC interval were written to a second file. In a third step we used a 20 min plot to display 3 s THEMIS  $V_{\perp x}$  and  $B_z$  in GSM coordinates, and the  $AL$  index at 1 min resolution. An example is presented in Figure 2. The times of peak flows determined previously were used to center Figures 2 (top) and 2 (bottom). With this program we identified the time of the initial flow burst in a BBF, the time of the beginning of  $B_z$  increase, and the time of the sharp break in the  $AL$  index. During this process we found many more short-duration drops in  $AL$  index that appeared to be negative spikes in the 14 h plots, but were obviously short negative bays at expanded scale as illustrated in Figure 2. Addition of these events to our previous list of  $AL$  onsets significantly increased the number of possible substorm onsets. Also, Figure 2 shows that the first burst in this sequence was not detected by our threshold criterion but the second burst was. In this case we chose the start time of the first burst and associated it with the initial dipolarization and the onset of the negative bay since it is clearly the beginning of the bursty bulk flow (BBF).

[27] The list of  $AL$  onsets and SMC intervals produced by these automatic and manual selection procedures provide the fundamental data used in subsequent analysis. The specific methods used are described in detail in section 5.

## 5. Statistical Results

### 5.1. Properties of the Ion Flow

[28] The interval from 1 December 2007 through 30 June 2008 was used to obtain a statistical description of the ion flows at THEMIS D everywhere on the nightside. Figure 3 presents cumulative probability distributions (cdfs) of the probability of exceeding the value on the abscissa. The line with blue “x”s is for earthward flows ( $V_{\perp x} > 0$ ) and the line with red circles is for tailward flows. The vertical dashed line represents the threshold used in this work to define a “fast flow.” The probability that an earthward flow sample exceeds the threshold of 150 km/s is about  $2 \times 10^{-3}$ ,

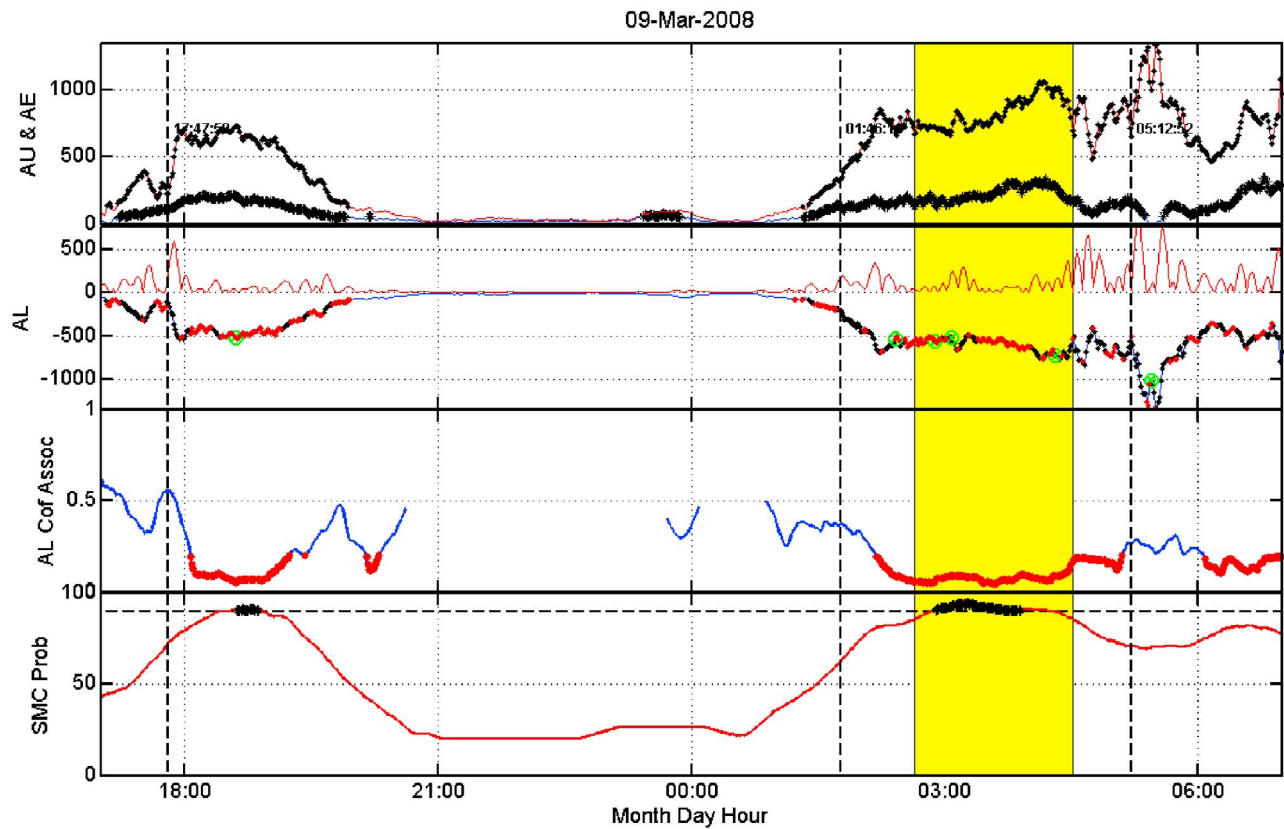


**Figure 1.** A plot of *AE* indices and quantities derived from them. The top panel displays the *AE* and *AU* indices with black asterisks showing points that satisfy the SMC criteria. The second panel shows the rectified filtered derivative of *AL* and the *AL* index. Red asterisks show *AL* values satisfying the SMC criterion. Black asterisks indicate that  $d(AL)/dt$  is not satisfied. The third panel shows the ratio of the running standard deviation to the running mean. Red asterisks denote possible SMC intervals. The bottom panel is a running count in a 90 min window of the number of times all SMC criteria are satisfied. Black asterisks denote times of possible SMC, as does the vertical patch, which was determined automatically by the program. Vertical dashed black lines indicate possible substorm expansion onsets.

a relative small value (0.2%), and the probability of a tailward flow over this threshold is about four times smaller. Earthward flows reach values in excess of 700 km/s while tailward flows never exceeded 300 km/s. Annotation on the graph shows the number of samples used to create these distributions (213 days), the percentage of fast flow events that were earthward (70.5%), and the percentage of 3 s samples greater than 150 km/s that were earthward (89.0%). The duration of the flows at THEMIS D is shown in Figure 4. The e-folding time for earthward flows is  $\sim 59$  s while that of tailward flows is shorter at  $\sim 25$  s. The probability distribution of separations between peaks of flow bursts (not shown) has a peak at 100 s with a long tail extending beyond 700 s. These peaks correspond to the separation of peaks in a single BBF and to the separation of BBFs.

[29] A dynamic cdf of  $V_{\perp x}$  is presented in Figure 5. This map is produced by a superposed epoch analysis of 43 tailward flow events using the time of peak tailward flow as epoch zero. At each epoch time we calculate a cumulative probability distribution of the flow velocity and characterize it in the final map by deciles (thin lines and colors) and quartiles (thick lines). A negative peak close to epoch zero is

evident, but more importantly this is preceded four minutes earlier by an earthward flow peak. A similar map (not shown) using the times of peak flow of the 279 earthward flow events has a weak negative peak several minutes after epoch zero. These results suggest that in general earthward flows precede tailward flows.

[30] The fast flows are generally associated with an increase in  $B_z$  as demonstrated in Figure 6. About 5 min before the peak of a fast flow,  $B_z$  begins to increase reaching a level 5 nT higher within 5 min after the flow. However, careful examination of individual events such as the one shown in Figure 2 reveal that the increase in  $B_z$  is actually much more rapid ( $\sim 1$ – $2$  min) and usually occurs in association with the first flow burst in a BBF. The smooth rise shown in Figure 6 is an artifact of using all flow bursts rather than only the first flow burst in the analysis.

## 5.2. Spatial Properties of the Ion Flow

[31] The dependence of the measured plasma flow velocity on distance behind the Earth is revealed in Figure 7. Events were chosen with the requirement that at least one of the five THEMIS spacecraft observed  $V_x$  (not  $V_{\perp x}$ ) exceeding



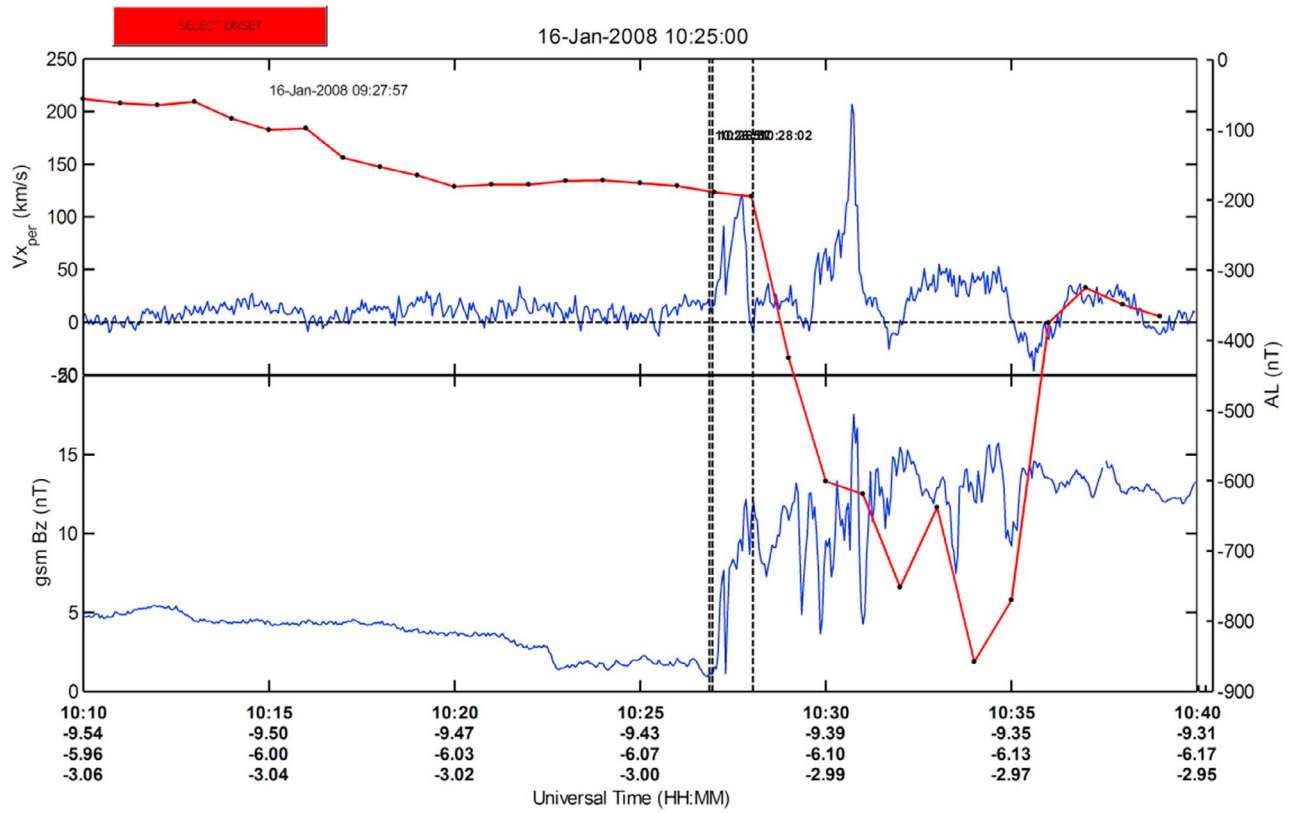


**Figure 2.** This shows (top) a plot of 3 s resolution GSM  $V_{\perp x}$  and (bottom) GSM  $B_z$ . The AL index at 1 min time resolution is overlain with its scale at right. The first vertical dashed line defines the onset of the first flow burst in this sequence and, in this case, the start of dipolarization. The sharp break in the AL index is closely associated with the first flow burst. Note this  $\sim 600$  nT negative bay lasts only 8 min.

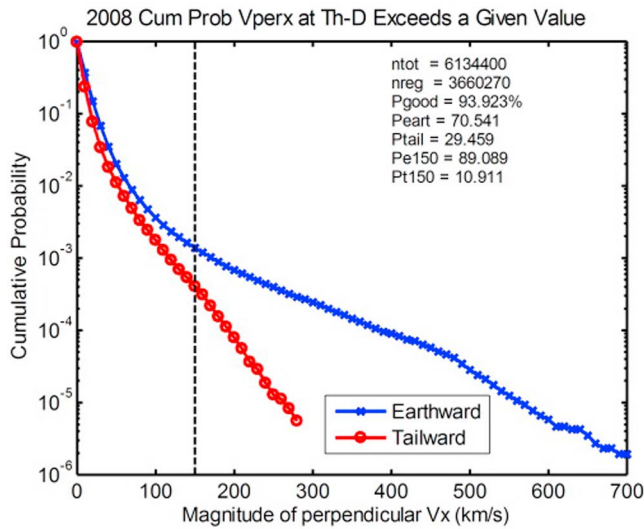


**Figure 3.** Cumulative probability distributions showing the probability that a given 3 s sample of the X component of the ion velocity perpendicular to the magnetic field exceeds the value shown on the abscissa. The blue line with “x”s is for earthward flow samples, and the red line with circles is for tailward flows. The vertical dashed line shows the threshold used to define “fast flow.”

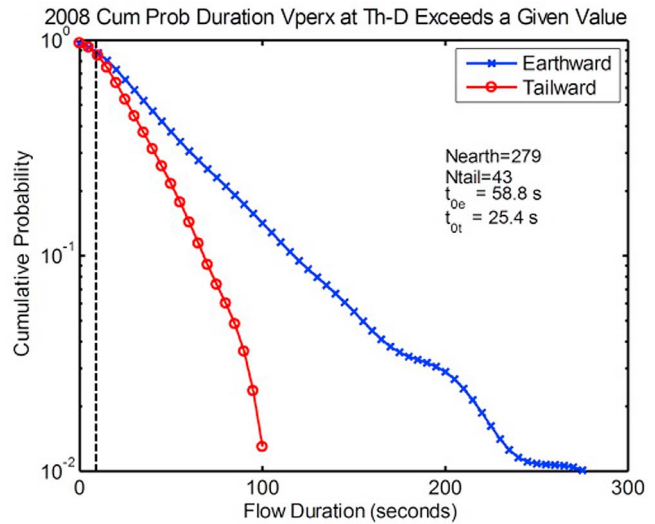


**Figure 4.** The cdfs of the duration of earthward and tailward ion flows at THEMIS D is shown. The line of blue “x”s is for earthward flows and is approximated by an exponential with e-folding times of  $\sim 59$  s. The line of red circles is for tailward flow and has an e-folding time of  $\sim 25$  s.

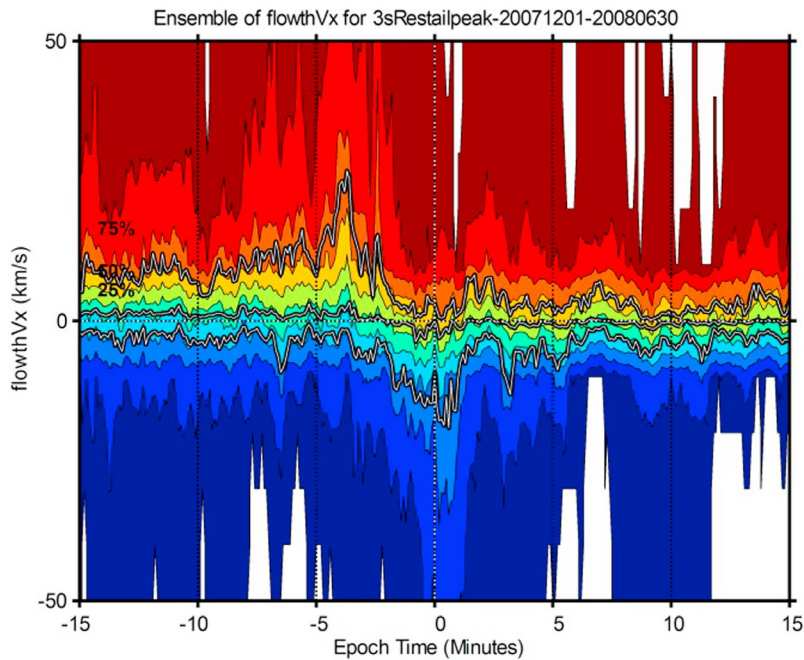


**Figure 5.** A superposed epoch analysis of  $V_{\perp X}$  is presented as a dynamic cdf. Contour lines and changes in color are drawn at deciles of the cdf. Quartiles are shown by the heavy lines. The time of peak tailward flow was used as epoch zero. Note that a peak in earthward flow typically occurs 4 min before the tailward flow.

150 km/s. For each such event the position of all spacecraft and the maximum values of  $V_x$  at each spacecraft around this time were recorded regardless of the magnitude of  $V_x$ . These results were then binned as a function of  $X$  GSM and

for each bin the deciles of the cdf of speed were determined. All observed speeds (along  $X$ ) are plotted in the diagram with smooth lines through the decile points in each bin. The results suggest that the flow speed is constant from near

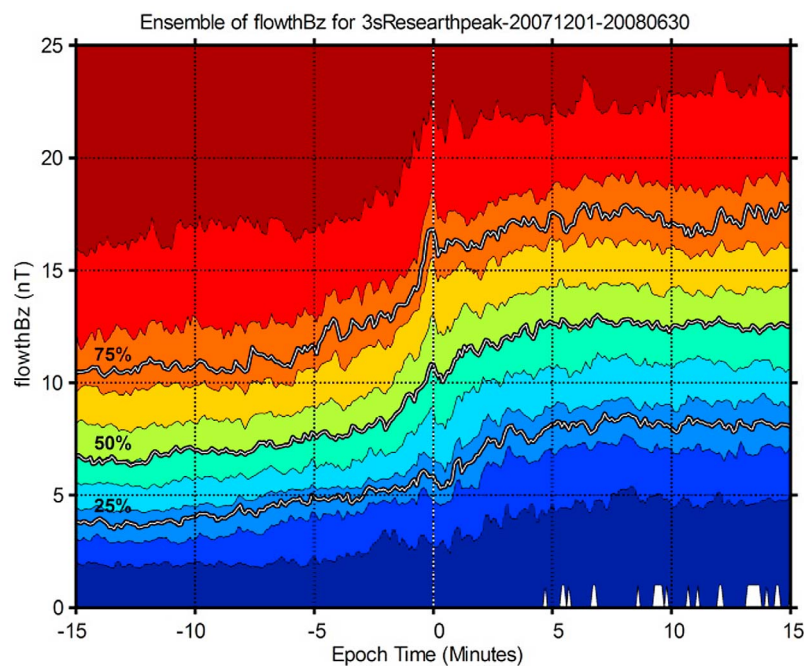


**Figure 6.** A dynamic cdf of the GSM  $B_z$  component at THEMIS D using the time of the peak in  $V_{\perp X}$  as epoch zero is presented. The decile lines show that  $B_z$  generally increases by about 5 nT in association with a peak in ion flow.



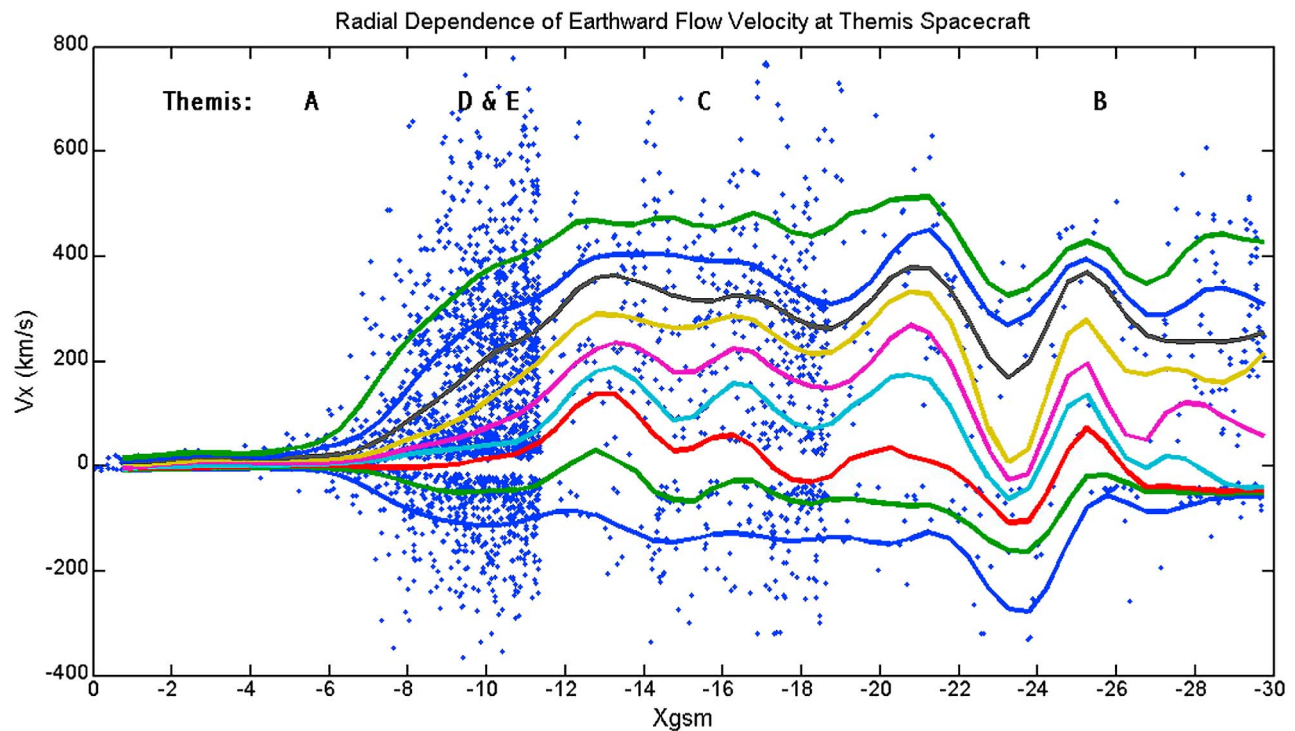


**Figure 7.** The peak earthward flow velocities at all five THEMIS spacecraft are shown for every event for which  $V_x$  (not  $V_{\perp x}$ ) at one or more spacecraft exceeds the threshold of  $V_x > 150$  km/s. Decile lines are shown for bins along the GSM  $x$  axis. From about  $22 R_E$  inward the lines indicate nearly constant velocity, but inside of  $12 R_E$  the speed rapidly decreases to zero by  $6 R_E$ .

$-22 R_E$  to  $-12 R_E$ . Closer to the Earth than this the flow along  $X$  decreases reaching zero speed at about  $-6 R_E$ . In addition there is an interesting change in the distribution of flow speeds beyond  $-22 R_E$ . From  $-22$  to  $-25 R_E$  the number of tailward flows increase relative to earthward flows. This location has been previously reported as the average location of the substorm  $X$  line.

[32] Figure 7 shows that the earthward flow speed decreases inside of  $12 R_E$ . THEMIS D has its apogee at  $R = 11.9 R_E$  and hence should observe this process clearly. In Figure 8 results for only fast flows ( $V_{\perp x} > 150$  km/s) at THEMIS D are plotted as a function of radial distance  $R$  in contrast to  $X$  GSM used in the preceding figure. Figure 8a presents the probability density function (pdf) for observation of earthward flows (blue “x”s) and tailward flows (red circles) in  $0.1 R_E$  bins as a function of  $R$ . Both distributions approach zero at  $9 R_E$  and peak at  $11.7 R_E$ . In actuality we expect the peak to be precisely at  $11.9 R_E$  because the spacecraft spends the most time at this radial distance. However, our calculation of the pdf is done with kernel smoothing which decreases the pdf when the kernel overlaps a sharp edge in the distribution. Figure 8b is the pdf for the time the spacecraft spent in each radial bin. This pdf is peaked at the same distance as the flow speed as expected. Figure 8c displays the probability of observing earthward and tailward flows normalized by the time spent in each radial bin. This graph gives the probability, not the pdf, so it shows that tailward flows (red circles) are relatively improbable compared to earthward flows and that both decrease to zero near  $8.5 R_E$ . Again this suggests that the

flows are decelerated or deflected at the inner edge of the plasma sheet.

[33] The local time distribution of the fast flows is presented in Figure 9 in the same format as Figure 8. The pdfs in Figure 9a show that the flows predominantly occur in the interval 2100–0100 local time (LT). The distribution of earthward flows (blue “x”s) is virtually identical to the distribution of auroral expansion onsets (grey dash-dotted line) as determined from IMAGE satellite data by Frey *et al.* [2004]. The auroral onsets and earthward flows are both peaked at 2300 LT. The distribution of tailward flows is clearly offset by 0.5 h toward dawn. The significance of this is not clear, but the result is supported by a superposed epoch analysis of  $V_{\perp y}$ . Its dynamic cdf (not shown) indicates that the upper quartile (duskward) is  $+24$  km/s while the lower quartile (dawnward) is  $-37$  km/s indicating a preference for dawnward deflection of the flow. For comparison the upper quartile of the earthward flow distribution superposed by peak time of earthward flow is over 200 km/s demonstrating that the flow is primarily decelerated and only slightly deflected. The pdf of time spent in each LT bin is plotted in Figure 9b. Because our study begins on 1 December 2007 and only considers points  $R > 6 R_E$  and  $X < 0$  there are very few samples near dawn because of the phasing of the THEMIS orbit. This does not appear to be a problem since there were many samples at 03 LT but the pdfs of flow observation are approaching zero.

[34] The behavior of the fast flows at THEMIS D is exhibited in Figure 10. To obtain this graph each fast flow vector was averaged over the duration of the interval in

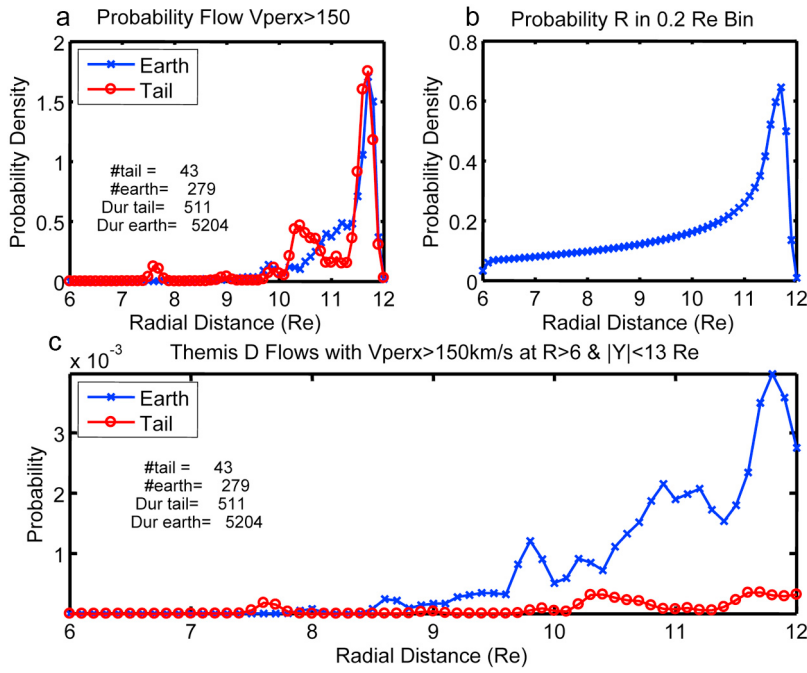


**Figure 8.** The probability of THEMIS D observing a fast flow event ( $V_{\perp x} > 150$  km/s) is presented. (a) The probability density function (pdf) for observation of earthward flows (blue “x”s) and tailward flows (red circles) in 0.1  $R_E$  bins as a function of radial distance from the Earth. (b) The pdf for the time the spacecraft spent in each radial bin. (c) The probability of observing earthward and tailward flows normalized by the time spent in each radial bin.

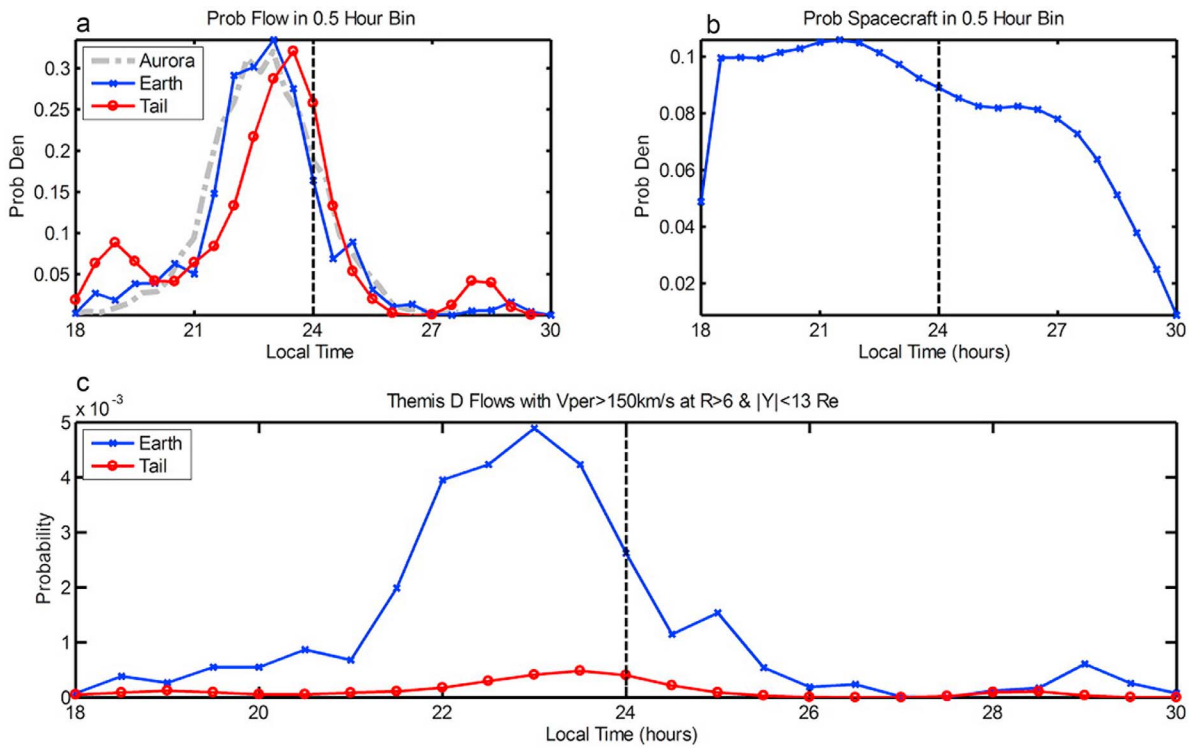


**Figure 9.** The local time (LT) distribution of fast flows is presented in the same format as in Figure 8. (a) The pdfs show the local time distribution of the two types of flows. In addition, the grey dash-dotted line shows the pdf for the local time occurrence of auroral onsets in IMAGE data. (b) The pdf shows the time the spacecraft spent in each LT bin during the study interval. (c) The probability of the two flow types as a function of local time.

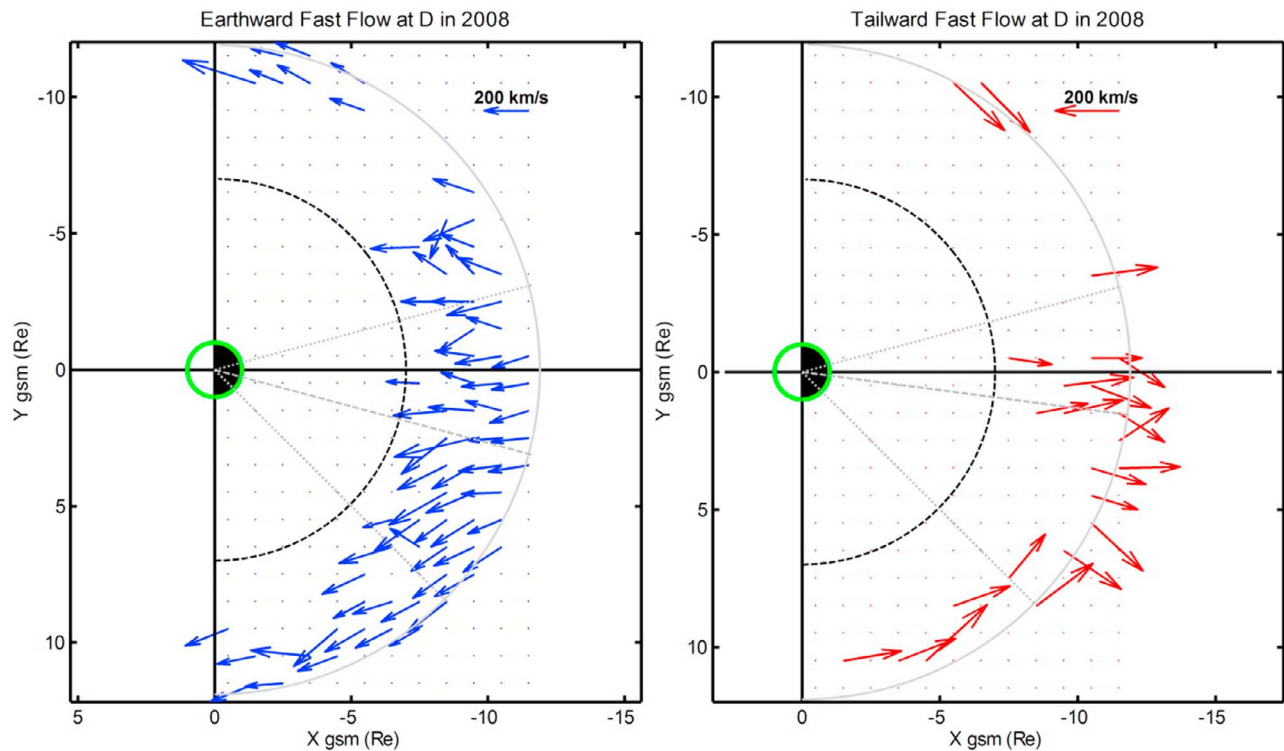


**Figure 10.** Fast flow vectors in  $1 R_E$  square bins were averaged and the vector plotted at the center of the bin. (left) Averages for 273 earthward flows and (right) averages for 42 tailward flows. The scale for velocity is shown in upper right of each frame. The grey dotted radial lines are the range of most frequent flows (2100–0100 LT), and the center grey dashed lines are the center of the two flow distributions.

which  $V_{\perp x}$  was above or below (tailward) the threshold. Then all flow vectors were assigned the location of the spacecraft at the peak of the flow burst and averaged in  $1 R_E$  square bins to obtain the average flow pattern in the GSM equatorial plane. Figure 10 (left) shows average earthward flows. The inner grey dashed semicircle is the inner limit of the study at  $7 R_E$ . The outer solid grey line is the apogee of THEMIS D at  $11.9 R_E$ . The grey dotted radial lines indicate the local time sector containing most of the flows. The grey dashed radial line is the center of the local time distribution. It is evident that plus or minus an hour of midnight the flows are almost directly sunward with only a minor azimuthal component. This is the region of deceleration and pileup of the earthward flows. At earlier local time the average flow vectors have an azimuthal component toward dusk suggesting flow around the Earth. Past 0100 LT the flow vectors are more erratic but have an azimuthal component toward dawn. Near the dawn terminator there are strong sunward flow vectors which are probably in the low-latitude boundary layer.

[35] Figure 10 (right) displays the average tailward flow vectors. They appear to divide into two classes. Close to both terminators the vectors are azimuthal toward midnight. Near midnight the second class of tailward flows is directly outward suggesting that the earthward flows have been turned around. At earlier local times there is a slight westward component to the tailward flows perhaps due to ion drifts. The peculiar nature of the first class of flows toward midnight requires further investigation.

[36] Properties of all perpendicular flow measurements observed by THEMIS D are summarized in Figure 11. The results plotted are derived from 4,789,570 three-second samples obtained on the nightside at GSM equatorial distances greater than  $6 R_E$ . Original flow and position data in GSM coordinates were transformed to an equatorial polar coordinate system  $[\rho, \text{LT}]$ . In this system the azimuthal flow angle of every measurement was determined as  $\text{angle} = \text{atan2}(v_{\phi}, v_{\text{rad}})$ . An angle of  $-90^\circ$  corresponds to westward motion of the plasma toward dusk and  $+90^\circ$  to eastward motion toward dawn. Data were then restricted to polar bins with dimensions  $0.5 R_E$  and 1 h LT. In each bin we calculated percentile lines of the distributions of  $v_{\text{rad}}$ ,  $v_{\phi}$ ,  $\text{angle}$ ,  $V_{\text{eq}} = \sqrt{V_x^2 + V_y^2}$ , and  $\text{ratio} = V_x/V_y$ . From the top down, Figure 11 shows percentile lines of three of these properties ( $v_{\text{rad}}$ ,  $v_{\phi}$ , and  $\text{angle}$ ) as a function of radial distance.

[37] Figure 11 (top) displays properties of the radial component of equatorial flow where positive values of  $v_{\text{rad}}$  are radially outward. Twelve traces above and 12 below the baseline correspond to 12 local time bins from 1800 to 0600 local time. The lines above correspond to the 99.999% value of the distribution and those below to the 0.001% value. The thick dashed black line with diamond markers show the radial profiles at midnight. The solid red lines with circles correspond to the dawn meridian, and the solid black lines with triangles correspond to the dusk meridian. Grey lines in between these sets of lines represent other local times.



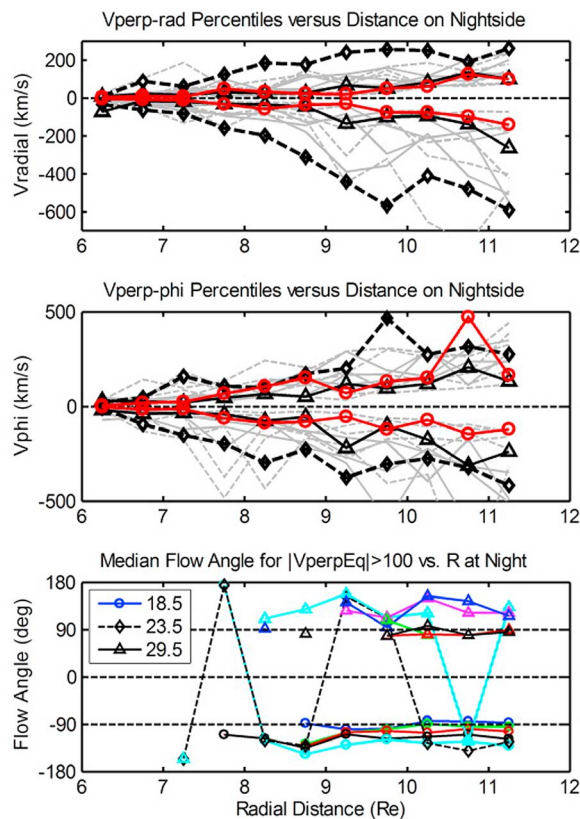


**Figure 11.** Properties of THEMIS D flow measurements as a function of local time and radial distance are presented. (top) The radial component (positive outward) of all flow measurements as a function of radial distance. Different traces correspond to different local times as explained in the text. (middle) The azimuthal component (positive toward dawn) versus radial distance and local time. (bottom) The azimuthal flow angle of only those flows having a GSM equatorial component exceeding 100 km/s. Positive angles are flow toward dawn.

[38] It is obvious from Figure 11 (top) that the highest earthward flows ( $v_{rad} < 0$ ) are observed near midnight in the hour centered at 2350 LT. Almost every earthward flow seen at other local times and the same radial distance is weaker than that seen near midnight. The same is true for reflected flows near midnight. While the outward flows ( $v_{rad} > 0$ ) are weaker than the earthward flows they are much faster near midnight than at other local times. Both Figures 11 (middle) and 11 (bottom) also show that no flow with speed greater than about 20 km/s penetrates inside of  $6 R_E$  at any local time. All of these facts suggest that earthward flows near midnight are decelerated and are either diverted to other local times or are reflected in both cases with much reduced speed.

[39] Figure 11 (middle) is identical in format to Figure 11 (top) and shows properties of the azimuthal component. Again the azimuthal flows near midnight (thick dashed black line with diamond markers) are larger than at other local times in agreement with the larger radial flows seen here. The azimuthal component decreases to zero inside of  $6 R_E$  at all

local times like the radial component. At the dawn and dusk terminators (traces close to baseline) the radial and azimuthal components are reduced to values of order 100–200 km/s. The azimuthal component is stronger than the radial component as might be expected for plasma flowing back to the dayside. There is a slight tendency for the near midnight plasma to preferentially flow toward dusk rather than dawn.

[40] Figure 11 (bottom) shows the median flow angle versus radial distance for all local times. Since most of the measurements are close to the noise level, we have restricted the analysis to only those flows with equatorial speed greater than 100 km/s. Even with this relatively weak constraint there are very few flows of this magnitude observed inside of  $8 R_E$ . Only near midnight (dashed black line) are such flows seen inside  $7.5 R_E$ . For those flows that exceed this limit the different traces show the median flow angle as a function of radial distance and local time. The traces fall into two sets: postmidnight with angle  $> 90^\circ$  and premidnight with angle  $< -90^\circ$ . In both sets the median flow angle indicates that the plasma is slowly approaching the Earth as it flows from midnight toward the terminators. In other words, there is a slight inward radial flow combined with azimuthal flow. Only near midnight is the flow pattern confused with a tendency to flow in either direction.

[41] These flow data suggest that during substorms plasma is injected between 2100 and 0100 local time. As the plasma approaches synchronous orbit it is decelerated and either deflected or diverted around the Earth. In the hour before local midnight the plasma may be diverted in either direction or reflected but premidnight it is preferentially diverted toward dusk and postmidnight it is diverted toward dawn. As the plasma flows toward the terminators it moves into regions of stronger field and slows considerably from its initial values seen near midnight.

### 5.3. Solar Wind Driver of Ion Flows

[42] A dynamic cdf of  $E_s = VB_s$  is displayed in Figure 12. A 6 h interval centered on the time of peak earthward flow was used with epoch zero at the time of peak flow. About half of the data points correspond to northward IMF and were set to zero. Consequently, many deciles have collapsed onto the base line when IMF  $B_z$  is northward ( $E_s = 0$ ). About 70 min before the peak of the fast flow (epoch zero) the IMF turns southward and median  $E_s$  rises above the baseline. Shortly before the fast flow the IMF turns northward as evidenced by the sudden drop in the median and upper quartile. This behavior precedes many substorm onsets and is commonly referred to as substorm triggering. In section 5.4 it is shown that a sudden decrease in  $AL$  is also associated with the peak of fast flows at THEMIS D.

### 5.4. Response of Substorm Indices to Fast Flows

[43] In the discussion of Figure 1 we showed an example of the 14 h long plots used to select sharp breaks in the  $AL$  index. In this initial survey we looked for a sudden increase in the magnitude of the  $AL$  derivative (red trace in second panel), a sudden onset of a decrease in the trace of the  $AL$  index (black asterisks on lower trace in second panel), and a peak in the 15 min running ratio of the standard deviation to the running mean of  $AL$ . This initial survey found 893  $AL$  onsets. Subsequently, a 20 min interval centered on the time

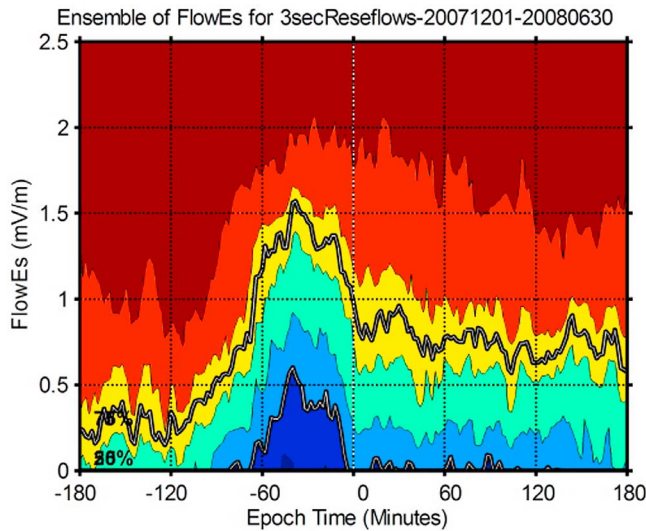


**Figure 12.** The dynamic cdf of the rectified solar wind electric field ( $E_s = VB_s$ ) is shown here for the 279 earthward flow events. Positive  $E_s$  corresponds to southward IMF  $B_z$ . Epoch zero is the time of peak fast flow at THEMIS D. Intervals of northward IMF ( $E_s = 0$ ) are included in the cdf so many deciles have collapsed onto the base line.

of fast flows was used to refine the onset timing and to associate fast flows with possible  $AL$  onsets. This survey provided more accurate timing and identified a number of additional negative bays of shorter duration. The final refined list contained 972  $AL$  onsets, about three times the number of fast flows observed. Many of these onsets occurred sunward of the  $7 R_E$  boundary used to define flows or when the spacecraft was at local times where flows are less frequent. Thus, the ratio should not be taken as evidence that not all onsets are related to fast flows.

[44] A pdf of the time between  $AL$  onsets was calculated (but not shown here) for the initial and refined  $AL$  onsets. In the initial list there was a broad peak at about 3 h. Using the refined list the final pdf was bimodal with a peak at 35 and 170 min. Most of the additional  $AL$  onsets in the refined list were short-duration negative bays superposed on the longer-duration bay found in the initial survey. It is these that are primarily responsible for the shorter time separations.

[45] The relation between flows and  $AL$  onsets was examined using the initial list of  $AL$  onsets and the peak times of all 322 fast flow bursts. The result was a broad distribution with nearly zero mean but a large standard deviation. An examination of some of these events revealed that it is the first flow burst in a sequence of flow bursts that appears to be associated with the  $AL$  onset, as was evident in Figure 2. This fact motivated the second survey using short intervals of 30 min duration. In this refined survey only the delay between the first flow burst and an  $AL$  onset was determined. Note that in many cases the first flow burst in a sequence previously identified had a peak magnitude well above background but below the threshold of 150 km/s. This onset of a flow was selected regardless of the peak magnitude. This procedure reduced the list of 322 flow bursts by about

half to 178 flow events. Five of these could not be associated with an  $AL$  onset within the 30 min range of the plot.

[46] The results of these calculations are shown in Figure 13. The initial survey produced a pdf with nearly zero mean delay ( $-3.4$  min), but a standard deviation of about 22 min as shown by the blue line of “x”s. All fast flows both earthward and tailward were associated with the nearest  $AL$  onset no matter how long delayed. However, the pdf and statistical properties were calculated for only those flow events with delays less than 60 min. In contrast the delay between the  $AL$  onsets in the refined survey and the first flow burst in a sequence of bursts is sharply peaked as demonstrated by the red line of circles. Many of the fast flows in the auto determination list were not the first flow in a sequence and were ignored in the refined survey. In total there were 173 initial flow bursts that could be associated with an  $AL$  onset. The pdf for this subset has a mean of  $-1.76$  min ( $AL$  before the flow) and a spread of 3.62 min. Taking into account the inherent inaccuracy of the  $AL$  index in substorm timing these distribution indicate that the arrival of the first flow at THEMIS D and the substorm onset are virtually simultaneous.

[47] The onset of the first flow burst in a list of 173 events associated with  $AL$  onsets was used to define epoch zero in a superposed epoch analysis of the  $AL$  index. The resulting dynamic cdf is shown in Figure 14. About 1 h before the flow burst the  $AL$  index begins to decrease. At the time of the flow burst there is a sudden increase in rate of decrease of  $AL$  evident in all deciles. This indicates that the response of the westward electrojet to the arrival of a fast flow inside  $11.9 R_E$  is a sudden increase in strength.  $AL$  reaches a minimum in 15–20 min and then between 30 and 40 min it begins to recover. By 90 min it has reached a relatively constant but nonzero value. A similar analysis using all 322 fast flow events produced a similar dynamic cdf but with a

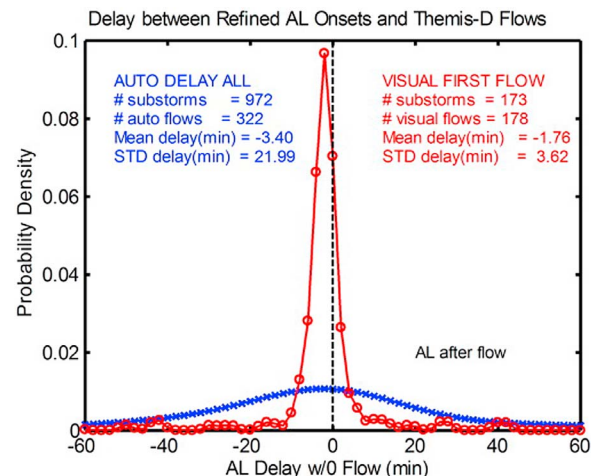


**Figure 13.** The pdfs for the delay between the onset time of a flow burst in  $V_{\perp x}$  and an  $AL$  onset are shown. The blue curve with “x”s is for an initial list of onsets and all fast flows. The red curve with circles is for a refined list using only the time of the first flow burst in a sequence of flow bursts. Annotations on the left and right show properties of these distributions.



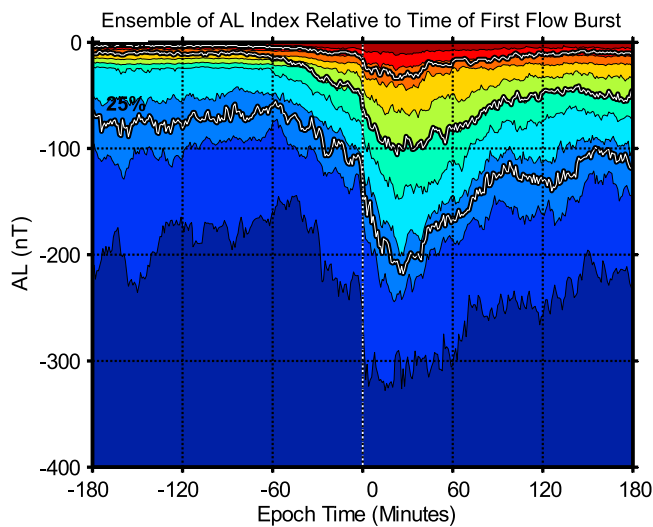


**Figure 14.** Superposed epoch analysis of the  $AL$  index for 173 fast earthward flow events selected from a list of 279 by the restriction that they are the first flow burst in a sequence of bursts. Epoch zero is the start of the first flow burst.

less sudden change in slope. This is to be expected as many of these events were not the initial flow burst in a sequence and were delayed by as much as 15 min from the onset of the first burst.

### 5.5. Relation of Fast Flows to Steady Magnetospheric Convection

[48] Steady magnetospheric convection (SMC) events were identified as described in the discussion of Figure 1. The procedure basically searches for intervals of elevated and relatively constant  $AE$  during which there is no evidence of a sudden decrease in the  $AL$  index. The indices must continuously exhibit this behavior for at least 90 min to be selected. Ninety-four intervals satisfying the SMC criteria were identified and their start times used as epoch zero in a superposed epoch analysis. A dynamic cdf of  $AE$  is presented in Figure 15 for these events. About 75 min before the selected start time  $AE$  begins to increase reaching a maximum at zero epoch time. Thereafter median  $AE$  remains at a relatively constant value of 250 nT for more than 90 min.

[49] A superposed epoch analysis of the IMF  $B_z$  (not shown) shows that median  $B_z$  becomes negative about 2 h before the start of the SMC, reaches a constant value of about  $-1.25$  nT 60 min before, and then remains almost constantly negative for the 2 h after the start. Medians of other solar wind parameters are constant through the 4 h of the dynamic cdfs. Characteristic solar wind values are:  $V \sim 500$  km/s,  $Den \sim 2.5$   $\text{cm}^{-3}$ ,  $B_{tot} \sim 4.5$  nT,  $E_s \sim 0.8$  mV/m (ignoring zeros). At THEMIS D the inclination of the magnetic field is constant at around  $25^\circ$ , density is around  $0.5$   $\text{cm}^{-3}$ , and  $Asym-D$  is constant, as are all the  $AE$  indices. The stability of all of these parameters provides confidence that SMC events have been correctly identified.

[50] To determine whether fast flows are associated with SMC the number of fast flow events before, during, and after SMC intervals were counted. For each event the

duration of the intervals before and after the SMC were set equal to the duration of the SMC. The initial result for 94 SMC was 17 before, 4 during, and 13 after. This surprising result prompted a detailed examination of the four events. It was found that all four were either bad data or the start and stop times were incorrectly identified so that the interval included a substorm expansion. In addition it was discovered that 20 of the SMC events occurred at times when the THEMIS D spacecraft was near apogee and close to or sunward of the dusk terminator. This is a region not considered in the auto detection of fast flows because of the possibility of contamination by boundary layer effects. When these events were eliminated leaving 74 events the three intervals contained 10, 1, and 7 earthward flow events, respectively. These results clearly suggest that that few or no fast flows are observed by THEMIS D during SMC events!

[51] The relation of SMC to plasma flows was also investigated with superposed epoch analysis. A dynamic cdf of  $V_{Lx}$  using the SMC start times as epoch zero was calculated. The 90% decile was only 20 km/s. Nowhere in the diagram was there evidence of any fast flow during the entire 4 h interval. Since 17 fast flow events were identified in the interval before epoch zero one can ask why they do not influence the contour lines in the dynamic cdf. The answer is that they do, but only at percentile levels above 98%. The events are randomly distributed relative to the start of the SMC and are of short duration ( $\sim 1$  min). In general no two events occur at the same epoch time and so there is a very low probability of a fast flow at any single epoch time. Clearly, if fast flows also occur randomly during SMC intervals they would not appear in the dynamic cdf for the same reason. The modified list of 74 SMC events was used to create a more sensitive display which is presented in Figure 16. The blue trace at the bottom is the 1%

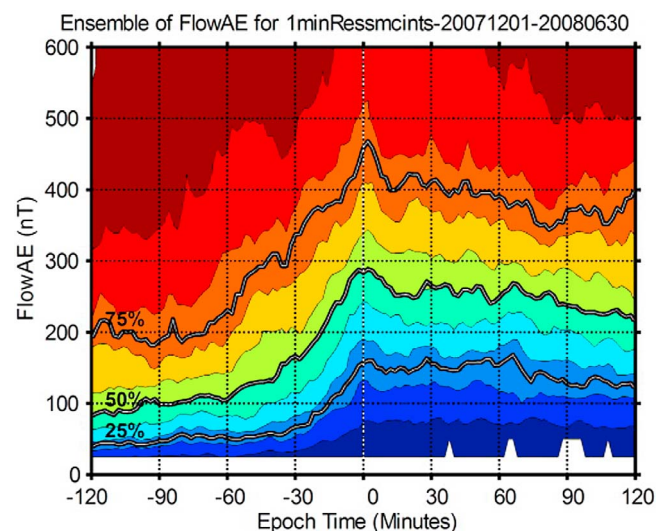


**Figure 15.** A superposed epoch analysis for a list of 94 steady magnetospheric convection (SMC) events during the 1 December 2007 to 30 June 2008 interval when THEMIS D passed through the tail. Epoch zero was taken as the apparent start time of the SMC which by definition lasts for 90 min or longer.

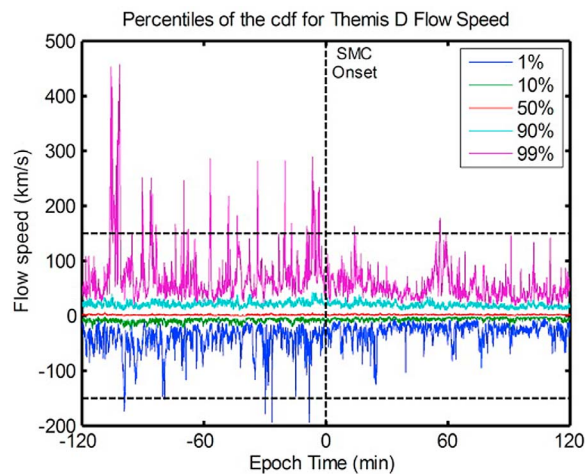


**Figure 16.** A superposed epoch analysis of  $V_{\perp x}$  with epoch zero defined by the start time of 74 SMC events. The presence of flow is only evident at the 1% level. More flows are seen before than during the SMC.

line and the purple trace at the top is the 99% line. It is obvious that the left and right side of the diagram differ considerably. Before the SMC onset there are numerous fast flows while after few flows exceed the threshold of 150 km/s. The actual number of events is 25 before and six after. If we shorten the interval after onset from 2 h to 90 min to correspond to the typical duration of SMC there are only four events after onset. This result validates the statement made above that fast flows rarely if ever penetrate inside of  $12 R_E$  during SMC.

[52] It should be noted that some fast flows were observed during SMC when THEMIS D was near the dusk terminator. In some cases these were long-duration tailward flows in the outer edge of the low-latitude boundary layer. In several other cases there were brief bursts of sunward flow but without the dipolarization characteristic of substorms near midnight. For the interval studied there were not a sufficient number of observations near dawn to determine whether a similar phenomenon occurs there.

## 6. Summary of Results

[53] It has been demonstrated that fast flows ( $V_{\perp} > 150$  km/s) are quite common at THEMIS D with  $\sim 322$  events identified in a six month interval. Fast flows are most frequently observed in the local time sector 2100–0100 h and at radial distances beyond  $8 R_E$ . Cumulative probability distributions (cdf) of the  $X$  component of the flow from all THEMIS spacecraft show that deciles of the cdf are constant from about  $22 R_E$  to  $12 R_E$  and then rapidly decrease to zero by synchronous orbit. Tailward flow events with  $V_{\perp} > 150$  km/s occur about 30% of the time but are of shorter duration and slower speed than earthward flows and occur in only 11% of the samples during fast flow events. Tailward flows rarely occur before an earthward flow but often occur alone. Peaks in both earthward and tailward fast flow bursts are associated with an increase in the GSM  $Z$  component of the magnetic field (dipolarization). Median IMF  $B_z$  is negative prior to fast flow events and decreases in

magnitude just before the event (northward turning). A sudden decrease in the  $AL$  index (pseudo breakup, substorm onset, or intensification) occurs at the time the first fast flow burst in a sequence of bursts (BBF) arrives at THEMIS D. The behavior of fast flows during steady magnetospheric convection events is very different from that seen at THEMIS D during substorms. During 74 SMC intervals only one fast flow burst was observed! A superposed epoch analysis finds very few fast flows above threshold after SMC onset implying that fast flows rarely if ever penetrate inside  $11.9 R_E$  during SMC.

## 7. Discussion

[54] The magnetosphere responds to a southward interplanetary magnetic field (IMF) in a variety of modes including pseudo breakups, expansion onsets, expansion intensifications, poleward boundary intensifications (PBI), steady magnetospheric convection (SMC), and sawtooth events [McPherron *et al.*, 2008]. The work reported here examines two of these response modes, substorm expansion onsets and SMC. Since only the  $AE$  indices have been used to define the start times of these events the possibility that some pseudo breakups, intensifications, and PBI are included in the event list cannot be ruled out. However, superposed epoch analysis of the  $AL$  index for the event lists reveals the standard response [Weimer, 1994] expected during substorms: 1 h long growth phase, 10–30 min expansion phase, and 90 min recovery phase. Since pseudo break ups, intensifications, and PBI generally occur 10–30 min apart multiple times during a single substorm [Hsu and McPherron, 2007; Rostoker, 1968], a predominance of such events in the list would smooth the median behavior of the  $AL$  index so that the expected behavior would not be observed. We conclude that most of the events have been correctly identified as expansion onsets. However, in this discussion we refer to these as  $AL$  onsets indicating the sudden development of a westward electrojet in the midnight sector.

[55] In recent work it has been demonstrated that each one of the response modes is associated with the closure of open magnetic flux in the tail, that is, that magnetic reconnection plays an important role in these phenomena [Hubert *et al.*, 2006, 2008; Milan *et al.*, 2003, 2007]. Furthermore, to the resolution of the analysis ( $\sim 12$  min) flux closure and the expansion onset are simultaneous. In our study we find that both the  $AL$  onsets and the start time of SMC intervals are associated with a predominantly southward IMF  $B_z$  indicating that dayside reconnection is occurring during the events. This implies that there is excess open flux in the tail lobes and we assume that the magnetic activity we observe is a consequence of reconnection in the tail.

[56] The primary focus of this study is the properties of fast flows at the inner edge of the plasma sheet ( $R < 11.9 R_E$ ). Fast flow was defined as  $V_{\perp x} > 150$  km/s even though higher values have been used in the past [Angelopoulos *et al.*, 1992; Baumjohann *et al.*, 1990]. Several studies have attempted to measure the width of these flow channels and the conclusion is that they are only a few  $R_E$  wide otherwise too much magnetic flux would be transported to the inner magnetosphere [Angelopoulos *et al.*, 1992; Nakamura *et al.*, 2005]. The only known process that creates narrow, high-speed flow channels in the tail is transient, localized, magnetic

reconnection. High-resolution MHD simulations clearly show that this is the normal behavior of the tail once reconnection begins [Ashour-Abdalla et al., 2002; Walker et al., 2006; Wiltberger et al., 2000]. Other processes that stimulate earthward flow such as dayside reconnection or instability of the plasma near midnight at 8–12  $R_E$  should produce a rarefaction wave that stimulates a broad region of slow flow toward the dayside. We assume that the high-speed flows we observe with THEMIS D at the inner edge of the plasma sheet are produced by reconnection. It is important to recognize that this has not been established in the current study but the association of the observed flows with southward IMF  $B_z$  is consistent with this assumption.

[57] An important finding in this study is that fast flows appear to originate at 22  $R_E$  or beyond and travel earthward with relatively constant velocity. But at 12  $R_E$  the flows begin to decelerate along the  $x$  axis, and by 8  $R_E$  no fast flows are observed. By 6  $R_E$  all inward flows have come to a stop although they continue azimuthally at greater distances. This suggests that inside 12  $R_E$  the flows encounter forces that slow and divert the flows. Shiokawa et al. [1997] have previously discussed this possibility and developed the idea that reconnection flows “pileup” near midnight in the outer magnetosphere. With our definition of fast flows we find that no flows with  $V_{\perp} > 150$  km/s penetrate inside of 8  $R_E$  during the first tail pass of THEMIS D. Previous studies using a higher threshold have found the inner edge of the flows to be further out [Angelopoulos et al., 1994], a result consistent with our observation of deceleration inside of 12  $R_E$ .

[58] In this study we found that 30% of the fast flow events are tailward when measured by event count. However, the tailward flows have less than half the duration of earthward flows and account for only 11% of the time in fast flows. The cumulative probability distribution of flow speeds is quite different for earthward and tailward flows. Earthward flows can exceed 800 km/s but tailward flows rarely exceed 300 km/s. Both earthward and tailward flows are associated with dipolarization of the local magnetic field (prolonged increase in  $B_z$ ). That earthward flows do this is easily understood as a flow perpendicular to the magnetic field indicates that the plasma is carrying magnetic flux from the outer tail. Taken together the properties of the tailward flows suggest that they are produced by reflection or vorticity in the pileup region. A similar conclusion was reached by Baumjohann et al. [2002].

[59] To examine the relation of the fast flows to substorm and SMC activity we created lists of all  $AL$  and SMC onsets in the interval 1 December 2007 to 30 June 2008. The initial substorm list was produced by a scan of 14 h panels centered at 0000 and 1200 UT. Visual selection of sharp onsets of a decrease in  $AL$  produced a total of 893 in the 7 month interval. Subsequently, we refined this list using the times of peak earthward flow as the center of 20 min panels. In these panels we found a number of additional sharp breaks in  $AL$  slope that increased the number of  $AL$  onsets to 972. Since we did not examine intervals without flows it is likely that the list of  $AL$  onsets should be larger still. However, our objective was to correlate  $AL$  onsets with flow onsets so the refined list corresponds to  $AL$  onsets close to a fast flow onset. In creating the refined list of  $AL$  onsets we found that the best correlation between  $AL$  onsets and fast flow onsets is with the first flow burst in a sequence of fast flow bursts, that is,

within a single bursty bulk flow (BBF). Flow bursts later in the sequence are obviously associated with the  $AL$  onset but with a larger delay than the first flow burst. In many cases we found that the first flow burst did not pass our velocity threshold although a later flow burst did. We took the beginning of the first flow burst as the relevant time regardless. The peak velocity in these bursts was well above background and from the distribution of flow speeds any particular threshold is arbitrary.

[60] We used both the initial and refined lists of  $AL$  onsets to determine the separation between substorm onsets. The distribution was bimodal with peaks at 35 and 170 min. The 170 min peak corresponds to the often reported 3 h separation of substorms [Borovsky and Nemzek, 1994; Borovsky et al., 1993; Prichard et al., 1996], while the 35 min peak is closer to the separation between pseudo breakups and PBI [Hsu and McPherron, 1998; Rostoker and Samson, 1981; Zesta et al., 2000]. A 12 h plot of  $B_z$  at THEMIS D reveals frequent dipolarizations of the magnetic field with the same time separation as these  $AL$  onsets. Clearly if the 3 h duration of a substorm has meaning then one substorm usually includes several BBFs carrying magnetic flux toward the Earth.

[61] We also examined the time delay between  $AL$  onsets and the initial flow burst in a BBF. Using our initial survey of 279 earthward flow bursts the distribution was centered close to zero delay but had a very large spread with standard deviation of about 22 min. However, when we used only the first flow burst in a BBF (173 events) we found the distribution was sharply peaked near zero delay with a standard deviation of only 3 min. It is interesting to note that both distributions were actually centered 2–3 min before the flow onsets. If these mean delays are physically meaningful they suggest that the substorm current wedge begins before the arrival of the flow at THEMIS D. This appears to support the view of advocates of the current disruption theory that flows are created by the current wedge. However, an alternative explanation is that effects of the flow are propagated to the Earth by Alfvén waves from regions outside 12  $R_E$  and that the current wedge is beginning to flow through the ionosphere even as the flow arrives at THEMIS D. Another possibility is that the THEMIS D observations are biased by the spacecraft often being outside the local time sector of substorm onset and the arrival of flows in these regions is delayed. Still another alternative is that the  $AL$  index is an inaccurate measure of expansion onset time. However, we would expect the detection of electrojet signatures in  $AL$  to be delayed relative to its formation. The detailed interpretation of these mean delays requires more accurate determination of substorm onset times and knowledge of the location of the spacecraft relative to the substorm current wedge. Nonetheless these results establish that an enhancement of the westward electrojet is associated within a minute or two with the initial arrival of a sequence of flow bursts at the inner edge of the plasma sheet.

[62] Our examination of the local time distribution of fast flows at THEMIS D showed that they most frequently occur between 2100 and 0100 local time. This distribution is virtually identical to that seen in satellite images of auroral expansion onset as was shown in Figure 9. This similarity suggests that there is a causal relation between the arrival of a fast flow in the inner magnetosphere and the expansion

phase of an auroral substorm. The association of dipolarization and the onset of a negative bay with the arrival of the flow also suggest that there is a causal relation between the flows and these phenomena.

[63] An interesting fact obvious in our data is that the local time distribution of tailward flows is offset by 0.5 h toward dawn from the earthward flow distribution. This offset is consistent with the observation that the quartile of  $V_{\perp X}$  in the dawnward direction (37 km/s) is larger than the quartile in the duskward direction (24 km/s). There is no obvious reason for this offset but it must indicate a pressure distribution during substorms that preferentially reflects earthward flows toward dawn.

[64] The initial list of 893 *AL* onsets was used as epoch zero in a superposed epoch analysis of the IMF  $B_z$ . The dynamic cdf (not shown) has a minimum in  $B_z$  at the time of the *AL* onset indicating a northward turning about this time. We repeated this analysis with the subset of earthward flows using  $E_s = VB_s$  with the time of peak flows as epoch zero (Figure 12). We found that the flow was preceded by a sharp decrease in the strength of  $E_s$  a few minutes before the fast flow. This result suggests that a northward turning of the IMF triggers reconnection in the tail, a fast flow into the outer magnetosphere, and the onset of a substorm expansion. Since we showed that the arrival of a fast flow is associated within minutes with an *AL* onset, this result is consistent with previous reports that northward turnings trigger substorm onsets [Hsu and McPherron, 2002, 2003].

[65] Finally, we examined the association between the start of fast flows and the beginning of dipolarization. We found that the first flow burst is clearly associated with a sharp increase in  $B_z$ , but that subsequent flow bursts do not significantly increase the field strength. They do, however, seem to enhance the fluctuations in  $B_z$ . We attempted to determine which occurs first, the flow or the dipolarization. We found many clear cases arising from background where the flow appears to begin before the dipolarization. However, most of the time perturbations present in the magnetic field prior to the dipolarization preclude an accurate determination of the start of the dipolarization. Statistically we found that the two events are simultaneous within  $\pm$  one minute. We believe that it is likely that the magnetic perturbations are caused by the arrival of the flow but our timing analysis is not sufficiently accurate to prove this point. Although not documented in the paper we also found that the minimum in THEMIS  $B_z$  prior to the fluctuating dipolarization, the so-called “explosive growth phase” is delayed by about one minute from the start of the fast earthward flow.

[66] Our search for fast flows during SMC events was quite revealing. Our results are consistent with the statement that fast flows never penetrate to  $12 R_E$  on the nightside during SMC events. Since we know that SMC are a consequence of balanced dayside and nightside reconnection we must ask where is the return flow from the nightside? One possibility is that it emerges from a steady X line over a broad region at such a slow velocity that it is undetectable by the time it reaches THEMIS D. A more likely explanation is that during SMC a region of high pressure exists behind the Earth and that transient and localized flows are deflected around the Earth at distances beyond  $12 R_E$ . This would imply that sunward flow bursts should be evident at the terminators during SMC. Unfortunately our original

choice of the study interval was such that we had no flow measurement near the dawn terminator. However, at the dusk terminator we did have data and found one or two sunward flow bursts. Unfortunately the low-latitude boundary layer is very dynamic and it is difficult to separate sunward flows due to the viscous interaction from sunward flows due to reconnection. Resolution of this problem will require future work.

## 8. Conclusions

[67] Two modes of magnetospheric response were investigated in this study: substorms and steady magnetospheric convection. Both are clearly associated with southward interplanetary magnetic field and hence must in some way be consequences of magnetic reconnection. Virtually all fast flows reaching inside  $12 R_E$  in the local time sector 2100 to 0100 h can be associated with a sudden and persistent drop in the *AL* index indicating a substorm expansion has taken place. These fast flows deposit magnetic flux in the outer magnetosphere increasing the magnetic field strength by a substantial amount. Presumably this flux was created by reconnection further out in the tail since the lobe field strength and the size of the polar cap are observed to decrease during substorms. Also, plasmoids and TCRs are observed moving tailward within a minute or two [Taguchi et al., 1998] of substorm onset and these can only be created by the formation of a second X line in the tail close to the Earth. During SMC we discovered that no fast flows penetrate inside of  $12 R_E$  on the nightside. However, SMC are caused by balanced reconnection so reconnection flows must occur somewhere. Presumably they are deflected around the Earth at distances greater than  $12 R_E$  and so are invisible to the THEMIS D spacecraft. It should be emphasized that when no flows penetrate to  $12 R_E$  there is no dipolarization of the nightside magnetic field, no rapid fluctuations in the magnetic field, and no sudden decreases in the *AL* index. It would appear that it is the arrival of the fast flow that creates these phenomena as reconnection is occurring both in substorms when these phenomena are present and in SMC when they are not.

[68] **Acknowledgments.** The authors thank the investigators responsible for the development, calibration, and processing of THEMIS magnetometer and plasma moment data. They also thank the individuals responsible for acquisition and distribution of solar wind and magnetic index data through the NASA NSSDC data center. Data analysis was supported by NASA grants NNX07AG16G and NNX07AF60G. The THEMIS PI was supported by NASA contract NAS5-02099.

[69] Masaki Fujimoto thanks Tuija Pulkkinen and another reviewer for their assistance in evaluating this manuscript.

## References

- Akasofu, S.-I. (1964), The development of the auroral substorm, *Planet. Space Sci.*, 12(4), 273–282, doi:10.1016/0032-0633(64)90151-5.
- Angelopoulos, V. (2008), The THEMIS Mission, *Space Sci. Rev.*, 141(1–4), 5–34, doi:10.1007/s11214-008-9336-1.
- Angelopoulos, V., W. Baumjohann, C. F. Kennel, F. V. Coroniti, M. G. Kivelson, R. Pellat, R. J. Walker, H. Lühr, and G. Paschmann (1992), Bursty bulk flows in the inner central plasma sheet, *J. Geophys. Res.*, 97(A4), 4027–4039, doi:10.1029/91JA02701.
- Angelopoulos, V., C. Kennel, F. Coroniti, R. Pellat, M. Kivelson, R. Walker, C. Russell, W. Baumjohann, W. Feldman, and J. Gosling (1994), Statistical characteristics of bursty bulk flow events, *J. Geophys. Res.*, 99(A11), 21,257–21,280, doi:10.1029/94JA01263.



- Angelopoulos, V., et al. (1996), Multipoint analysis of a bursty bulk flow event on April 11, 1985, *J. Geophys. Res.*, *101*(A3), 4967–4989, doi:10.1029/95JA02722.
- Ashour-Abdalla, M., M. El-Alaoui, F. V. Coroniti, R. J. Walker, and V. Peromian (2002), A new convection state at substorm onset: Results from an MHD study, *Geophys. Res. Lett.*, *29*(20), 1965, doi:10.1029/2002GL015787.
- Baker, D. N., T. I. Pulkkinen, V. Angelopoulos, W. Baumjohann, and R. L. McPherron (1996), Neutral line model of substorms: Past results and present view, *J. Geophys. Res.*, *101*(A6), 12,975–13,010, doi:10.1029/95JA03753.
- Baumjohann, W. (1988), The plasma sheet boundary layer and magnetospheric substorms, *J. Geomag. Geoelectr.*, *40*(2), 157–175.
- Baumjohann, W. (1996), Near-Earth plasma sheet dynamics, *Adv. Space Res.*, *18*(8), 27–33, doi:10.1016/0273-1177(95)00993-0.
- Baumjohann, W., G. Paschmann, N. Sckopke, C. Cattell, and C. Carlson (1988), Average ion moments in the plasma sheet boundary layer, *J. Geophys. Res.*, *93*(A10), 11,507–11,520, doi:10.1029/JA093iA10p11507.
- Baumjohann, W., G. Paschmann, and C. Cattell (1989), Average plasma properties in the central plasma sheet, *J. Geophys. Res.*, *94*(A6), 6597–6606, doi:10.1029/JA094iA06p6597.
- Baumjohann, W., G. Paschmann, and H. Lühr (1990), Characteristics of high-speed ion flows in the plasma sheet, *J. Geophys. Res.*, *95*(A4), 3801–3809, doi:10.1029/JA095iA04p3801.
- Baumjohann, W., G. Paschmann, T. Nagai, and H. Lühr (1991), Superposed epoch analysis of the substorm plasma sheet, *J. Geophys. Res.*, *96*(A7), 11,605–11,608, doi:10.1029/91JA00775.
- Baumjohann, W., M. Hesse, S. Kokubun, T. Mukai, T. Nagai, and A. Petrukovich (1999), Substorm dipolarization and recovery, *J. Geophys. Res.*, *104*(A11), 24,995–25,000, doi:10.1029/1999JA000282.
- Baumjohann, W., T. Nagai, A. Petrukovich, T. Mukai, T. Yamamoto, and S. Kokubun (2000), Substorm signatures between 10 and 30 Earth radii, *Adv. Space Res.*, *25*(7–8), 1663–1666, doi:10.1016/S0273-1177(99)00681-X.
- Baumjohann, W., R. Schodel, and R. Nakamura (2002), Bursts of fast magnetotail flux transport, *Adv. Space Res.*, *30*, 2241–2246, doi:10.1016/S0273-1177(02)80234-4.
- Birn, J., and M. Hesse (1991), The substorm current wedge and field-aligned currents in MHD simulations of magnetotail reconnection, *J. Geophys. Res.*, *96*(A2), 1611–1618, doi:10.1029/90JA01762.
- Birn, J., and M. Hesse (1996), Details of current disruption and diversion in simulations of magnetotail dynamics, *J. Geophys. Res.*, *101*(A7), 15,345–15,358, doi:10.1029/96JA00887.
- Birn, J., M. Hesse, G. Haerendel, W. Baumjohann, and K. Shiokawa (1999), Flow braking and the substorm current wedge, *J. Geophys. Res.*, *104*(A9), 19,895–19,903, doi:10.1029/1999JA000173.
- Borovsky, J., and R. Nemzek (1994), Comment on “The Earth’s magnetosphere under continued forcing: Substorm activity during the passage of an interplanetary cloud” by C. J. Farrugia, M. P. Freeman, L. F. Burlaga, R. P. Lepping, and K. Takahashi, *J. Geophys. Res.*, *99*(A8), 14,937–14,940, doi:10.1029/94JA00363.
- Borovsky, J. E., R. J. Nemzek, and R. D. Belian (1993), The occurrence rate of magnetospheric-substorm onsets: Random and periodic substorms, *J. Geophys. Res.*, *98*(A3), 3807–3813, doi:10.1029/92JA02556.
- Borovsky, J. E., M. Thomsen, G. D. Reeves, M. W. Liemohn, J. Kozyra, C. R. Clauer, and H. J. Singer (2001), Global sawtooth oscillations of the magnetosphere during large storms, *Eos Trans. AGU*, *82*(47), Fall Meet. Suppl., Abstract SM42D-08.
- Caan, M., D. Fairfield, and E. H. Jr. (1979), Magnetic fields in flowing magnetotail plasmas and their significance for magnetic reconnection, *J. Geophys. Res.*, *84*(A5), 1971–1976, doi:10.1029/JA084iA05p01971.
- Chapman, S. (1962), Earth storms: Retrospect and prospect, *J. Phys. Soc. Jpn.*, *17*(A-1), 6.
- de la Beaujardiere, O., L. R. Lyons, J. M. Ruohomemi, E. Friis-Christensen, C. Danielsen, F. Rich, and P. Newell (1994), Quiet-time intensifications along the poleward auroral boundary near midnight, *J. Geophys. Res.*, *99*(A1), 287–298, doi:10.1029/93JA01947.
- Frey, H. U., S. B. Mende, V. Angelopoulos, and E. F. Donovan (2004), Substorm onset observations by IMAGE-FUV, *J. Geophys. Res.*, *109*, A10304, doi:10.1029/2004JA010607.
- Henderson, M. G., et al. (2006), Substorms during the 10–11 August 2000 sawtooth event, *J. Geophys. Res.*, *111*, A06206, doi:10.1029/2005JA011366.
- Hesse, M., and J. Birn (1991), On dipolarization and its relation to the substorm current wedge, *J. Geophys. Res.*, *96*(A11), 19,417–19,426, doi:10.1029/91JA01953.
- Hones, E. W., Jr. (1973), Plasma flow in the plasma sheet and its relation to substorms, *Radio Sci.*, *8*(11), 979–990, doi:10.1029/RS008i011p0979.
- Hsu, T.-S., and R. L. McPherron (1998), The main onset of a magnetospheric substorm, in *Substorms-4: International Conference on Substorms-4, Lake Hamana, Japan, March 9–13, 1998, Astrophys. Space Sci. Libr.*, vol. 238, edited by S. Kokubun and Y. Kamide, pp. 79–82, Kluwer Acad., Dordrecht, Netherlands.
- Hsu, T.-S., and R. L. McPherron (2002), An evaluation of the statistical significance of the association between northward turnings of the interplanetary magnetic field and substorm expansion onsets, *J. Geophys. Res.*, *107*(A11), 1398, doi:10.1029/2000JA000125.
- Hsu, T.-S., and R. L. McPherron (2003), Occurrence frequencies of IMF triggered and nontriggered substorms, *J. Geophys. Res.*, *108*(A7), 1307, doi:10.1029/2002JA009442.
- Hsu, T.-S., and R. L. McPherron (2007), A statistical study of the relation of Pi 2 and plasma flows in the tail, *J. Geophys. Res.*, *112*, A05209, doi:10.1029/2006JA011782.
- Hubert, B., S. E. Milan, A. Grocott, C. Blockx, S. W. H. Cowley, and J.-C. Gérard (2006), Dayside and nightside reconnection rates inferred from IMAGE FUV and Super Dual Auroral Radar Network data, *J. Geophys. Res.*, *111*, A03217, doi:10.1029/2005JA011140.
- Hubert, B., S. E. Milan, A. Grocott, S. W. H. Cowley, and J. C. Gérard (2008), Open magnetic flux and magnetic flux closure during sawtooth events, *Geophys. Res. Lett.*, *35*, L23301, doi:10.1029/2008GL036374.
- Hubert, B., C. Blockx, S. E. Milan, and S. W. H. Cowley (2009), Statistical properties of flux closure induced by solar wind dynamic pressure fronts, *J. Geophys. Res.*, *114*, A07211, doi:10.1029/2008JA013813.
- Lui, A. T. Y. (1991), A synthesis of magnetospheric substorm models, *J. Geophys. Res.*, *96*(A2), 1849–1856, doi:10.1029/90JA02430.
- Lui, A. T. Y. (1996), Current disruption in the Earth’s magnetosphere: Observations and models, *J. Geophys. Res.*, *101*(A6), 13,067–13,088, doi:10.1029/96JA00079.
- Lui, A. T. Y., R. E. Lopez, S. M. Krimigis, R. W. McEntire, L. J. Zanetti, and T. A. Potemra (1988), A case study of magnetotail current sheet disruption and diversion, *Geophys. Res. Lett.*, *15*(7), 721–724, doi:10.1029/GL015i007p00721.
- Lui, A. T. Y., A. Mankofsky, C. L. Chang, K. Papadopoulos, and C. S. Wu (1990), A current disruption mechanism in the neutral sheet: A possible trigger for substorm expansions, *Geophys. Res. Lett.*, *17*(6), 745–748, doi:10.1029/GL017i006p00745.
- McPherron, R., C. Russell, and M. Aubry (1973), 9. Phenomenological model for substorms, *J. Geophys. Res.*, *78*(16), 3131–3149, doi:10.1029/JA078i016p03131.
- McPherron, R. L., J. M. Weygand, and H. Tung-Shin (2008), Response of the Earth’s magnetosphere to changes in the solar wind, *J. Atmos. Sol. Terr. Phys.*, *70*(2–4), 303–315, doi:10.1016/j.jastp.2007.08.040.
- Milan, S. E., M. Lester, S. W. H. Cowley, K. Oksavik, M. Brittacher, R. A. Greenwald, G. Sofko, and J. P. Villain (2003), Variations in the polar cap area during two substorm cycles, *Ann. Geophys.*, *21*(5), 1121–1140, doi:10.5194/angeo-21-1121-2003.
- Milan, S. E., G. Provan, and B. Hubert (2007), Magnetic flux transport in the Dungey cycle: A survey of dayside and nightside reconnection rates, *J. Geophys. Res.*, *112*, A01209, doi:10.1029/2006JA011642.
- Milan, S. E., P. D. Boakes, and B. Hubert (2008), Response of the expanding/contracting polar cap to weak and strong solar wind driving: Implications for substorm onset, *J. Geophys. Res.*, *113*, A09215, doi:10.1029/2008JA013340.
- Nakamura, R., et al. (2002), Motion of the dipolarization front during a flow burst event observed by Cluster, *Geophys. Res. Lett.*, *29*(20), 1942, doi:10.1029/2002GL015763.
- Nakamura, R., et al. (2005), Multi-point observation of the high-speed flows in the plasma sheet, *Adv. Space Res.*, *36*(8), 1444–1447, doi:10.1016/j.asr.2005.05.101.
- Nishida, A., and N. Nagayama (1973), Synoptic survey for the neutral line in the magnetotail during the substorm expansion phase, *J. Geophys. Res.*, *78*(19), 3782–3798, doi:10.1029/JA078i019p03782.
- Ohtani, S. (2004), Flow bursts in the plasma sheet and auroral substorm onset: Observational constraints on connection between midtail and near-Earth substorm processes, *Space Sci. Rev.*, *113*(1–2), 77–96, doi:10.1023/B:SPAC.0000042940.59358.2f.
- Ohtani, S., F. Creutzberg, T. Mukai, H. Singer, A. Lui, M. Nakamura, P. Prikryl, K. Yumoto, and G. Rostoker (1999), Substorm onset timing: The December 31, 1995, event, *J. Geophys. Res.*, *104*(A10), 22,713–22,727, doi:10.1029/1999JA000209.
- Ohtani, S., R. Yamaguchi, H. Kawano, F. Creutzberg, J. B. Sigwarth, L. A. Frank, and T. Mukai (2002a), Does the braking of the fast plasma flow trigger a substorm?: A study of the August 14, 1996, event, *Geophys. Res. Lett.*, *29*(15), 1721, doi:10.1029/2001GL013785.
- Ohtani, S. I., R. Yamaguchi, M. Nose, H. Kawano, M. Engbretson, and K. Yumoto (2002b), Quiet time magnetotail dynamics and their implica-



- tions for the substorm trigger, *J. Geophys. Res.*, *107*(A2), 1030, doi:10.1029/2001JA000116.
- Ohtani, S., M. A. Shay, and T. Mukai (2004), Temporal structure of the fast convective flow in the plasma sheet: Comparison between observations and two-fluid simulations, *J. Geophys. Res.*, *109*, A03210, doi:10.1029/2003JA010002.
- Ohtani, S., H. J. Singer, and T. Mukai (2006), Effects of the fast plasma sheet flow on the geosynchronous magnetic configuration: Geotail and GOES coordinated study, *J. Geophys. Res.*, *111*, A01204, doi:10.1029/2005JA011383.
- Ohtani, S., Y. Miyashita, H. Singer, and T. Mukai (2009), Tailward flows with positive  $B_z$  in the near-Earth plasma sheet, *J. Geophys. Res.*, *114*, A06218, doi:10.1029/2009JA014159.
- Prichard, D., J. Borovsky, P. Lemons, and C. Price (1996), Time dependence of substorm recurrence: An information-theoretic analysis, *J. Geophys. Res.*, *101*(A7), 15,359–15,369, doi:10.1029/95JA03419.
- Pytte, T., R. L. McPherron, E. W. Hones Jr., and H. I. West Jr. (1978), Multiple-satellite studies of magnetospheric substorms: Distinction between polar magnetic substorms and convection-driven negative bays, *J. Geophys. Res.*, *83*(A2), 663–679, doi:10.1029/JA083iA02p00663.
- Rostoker, G. (1968), Macrostructure of geomagnetic bays, *J. Geophys. Res.*, *73*(13), 4217–4229, doi:10.1029/JA073i013p04217.
- Rostoker, G., and J. C. Samson (1981), Polarization characteristics of Pi 2 pulsations and implications for their source mechanisms: Location of source regions with respect to the auroral electrojets, *Planet. Space Sci.*, *29*(2), 225–247, doi:10.1016/0032-0633(81)90036-2.
- Runov, A., V. Angelopoulos, M. I. Sitnov, V. A. Sergeev, J. Bonnell, J. P. McFadden, D. Larson, K.-H. Glassmeier, and U. Auster (2009), THEMIS observations of an earthward-propagating dipolarization front, *Geophys. Res. Lett.*, *36*, L14106, doi:10.1029/2009GL038980.
- Sergeev, V. A., R. J. Pellinen, and T. I. Pulkkinen (1996), Steady magnetospheric convection: A review of recent results, *Space Sci. Rev.*, *75*(3–4), 551–604, doi:10.1007/BF00833344.
- Sergeev, V., M. Shukhtina, R. Rasinkangas, A. Korth, G. Reeves, H. Singer, M. Thomsen, and L. Vagina (1998), Event study of deep energetic particle injections during substorm, *J. Geophys. Res.*, *103*(A5), 9217–9234, doi:10.1029/97JA03686.
- Shiokawa, K., W. Baumjohann, and G. Haerendel (1997), Braking of high-speed flows in the near-Earth tail, *Geophys. Res. Lett.*, *24*(10), 1179–1182, doi:10.1029/97GL01062.
- Shiokawa, K., W. Baumjohann, and G. Haerendel (1998a), Braking the high-speed flow and azimuthal pressure gradient as driving forces of substorm currents, in *Substorms-4: International Conference on Substorms-4, Lake Hamana, Japan, March 9–13, 1998*, *Astrophys. Space Sci. Libr.*, vol. 238, edited by S. Kokubun and Y. Kamide, pp. 355–360, Kluwer Acad., Dordrecht, Netherlands.
- Shiokawa, K., et al. (1998b), High-speed ion flow, substorm current wedge, and multiple Pi 2 pulsations, *J. Geophys. Res.*, *103*(A3), 4491–4507, doi:10.1029/97JA01680.
- Shiokawa, K., G. Haerendel, and W. Baumjohann (1998c), Azimuthal pressure gradient as driving force of substorm currents, *Geophys. Res. Lett.*, *25*(7), 959–962, doi:10.1029/98GL00540.
- Taguchi, S., J. Slavin, M. Kiyohara, M. Nose, G. Reeves, and R. Lepping (1998), Temporal relationship between midtail traveling compression regions and substorm onset: Evidence for near-Earth neutral line formation in the late growth phase, *J. Geophys. Res.*, *103*(A11), 26,607–26,612, doi:10.1029/98JA02617.
- Voronkov, I. O., E. F. Donovan, and J. C. Samson (2003), Observations of the phases of the substorm, *J. Geophys. Res.*, *108*(A2), 1073, doi:10.1029/2002JA009314.
- Walker, R. J., M. Ashour-Abdalla, M. E. Alaoui, and F. V. Coroniti (2006), Magnetospheric convection during prolonged intervals with southward interplanetary magnetic field, *J. Geophys. Res.*, *111*, A10219, doi:10.1029/2005JA011541.
- Weimer, D. (1994), Substorm time constants, *J. Geophys. Res.*, *99*(A6), 11,005–11,015, doi:10.1029/93JA02721.
- Wiens, R. G., and G. Rostoker (1975), Characteristics of the development of the westward electrojet during the expansive phase of magnetospheric substorms, *J. Geophys. Res.*, *80*(16), 2109–2128, doi:10.1029/JA080i016p02109.
- Wiltberger, M., T. Pulkkinen, J. Lyon, and C. Goodrich (2000), MHD simulation of the magnetotail during the December 10, 1996, substorm, *J. Geophys. Res.*, *105*(A12), 27,649–27,663, doi:10.1029/1999JA000251.
- Zesta, E., L. Lyons, and E. Donovan (2000), The auroral signature of earthward flow bursts observed in the magnetotail, *Geophys. Res. Lett.*, *27*(20), 3241–3244, doi:10.1029/2000GL000027.

---

V. Angelopoulos, X. Chu, T.-S. Hsu, J. Kissinger, and R. L. McPherron, Institute of Geophysics and Planetary Physics, University of California, 3845 Slichter Hall, PO Box 951567, Los Angeles, CA 90095-1567, USA. (rmcpherron@igpp.ucla.edu)